Synchronous helical pulse sequences in magic-angle spinning nuclear magnetic resonance: Double quantum recoupling of multiple-spin systems

Andreas Brinkmann, Mattias Edén, and Malcolm H. Levitt[a)]
Division of Physical Chemistry, Arrhenius Laboratory, Stockholm University, S-106 91 Stockholm, Sweden

(Received 6 December 1999; accepted 19 January 2000)

Some general principles of radio-frequency pulse sequence design in magic-angle spinning nuclear magnetic resonance are discussed. Sequences with favorable dipolar recoupling properties may be designed using synchronous helical modulations of the space and spin parts of the spin Hamiltonian. The selection rules for the average Hamiltonian may be written in terms of three symmetry numbers, two defining the winding numbers of the space and spin helices, and one indicating the number of phase rotation steps in the radio-frequency modulation. A diagrammatic technique is used to visualize the space-spin symmetry selection. A pulse sequence $C14_4^5$ is designed which accomplishes double-quantum recoupling using a low ratio of radio frequency field to spinning frequency. The pulse sequence uses 14 radio frequency modulation steps with space and spin winding numbers of 4 and 5, respectively. The pulse sequence is applied to the double-quantum spectroscopy of $^{13}C_3$-labeled L-alanine. Good agreement is obtained between the experimental peak intensities, analytical results, and numerically exact simulations based on the known molecular geometry. The general symmetry properties of double quantum peaks in recoupled multiple-spin systems are discussed. A supercycle scheme which compensates homonuclear recoupling sequences for chemical shifts is introduced. We show an experimental double-quantum ^{13}C spectrum of [U–^{13}C]–L-tyrosine at a spinning frequency of 20.000 kHz. © *2000 American Institute of Physics.* [S0021-9606(00)01214-9]

I. INTRODUCTION

Solid state nuclear magnetic resonance (NMR) may be used for determining local molecular structures in isotopically labeled biomolecules. Methods exist for determination of accurate intermolecular distances,[1–17] and molecular torsional angles.[18–24] The methods have been applied to systems such as noncrystalline membrane proteins[25] providing information which is currently inaccessible any other way.

Most realistic applications require rapid magic-angle spinning (MAS) in order to obtain maximal signal intensity and spectral resolution. Molecular structural information is obtained by applying radio frequency (rf) pulse sequences which implement temporary recoupling of the nuclear spin system, in order to take advantage of the dipole–dipole couplings between the nuclear spins. The radio frequency recoupling schemes may be incorporated into multidimensional procedures, leading to powerful methods for spectral assignment and geometry determination.[15,26–29]

Most of the existing recoupling methods fall into two broad classes, depending on whether they generate (in ideal circumstances) a zero-quantum or double-quantum average Hamiltonian for the recoupled spin pairs. For example, the rotational resonance,[1–6] RFDR,[26] and RIL[12] schemes are zero-quantum recoupling methods. The HORROR[13] and C7[14] schemes and their variants,[15–17] are double-quantum recoupling techniques. The DRAMA[9] and DRAWS[10] sequences produce mixtures of double-quantum and zero-quantum average Hamiltonians. These alternative modes of recoupling may be complementary, in the sense that they operate best in different circumstances. It has been pointed out[12] that evolution under a zero-quantum average Hamiltonian conserves the total longitudinal magnetization in multiple-spin systems, leading to a uniform distribution of magnetization at long mixing intervals. This corresponds to the solution-state TOCSY method,[30] which is very useful for assignment purposes. The double-quantum methods, on the other hand, allow the use of double-quantum spectroscopy to establish assignments, as in the solution-state INADEQUATE experiment,[31–33] at the same time as ensuring complete suppression of isolated spin signals, an important advantage in large biomolecules.

In addition, double-quantum techniques have been developed which are insensitive to one of the three Euler angles determining the orientation of molecules in a powder sample. This leads to high efficiency in nonoriented samples.[13,14] So far only rotational resonance[1–6] achieves this in the case of zero-quantum recoupling.

One of the technical problems affecting current double-quantum recoupling sequences is the need for high rf fields at the Larmor frequencies of the recoupled spin species (henceforth denoted by *S*). For example, the C7,[14] POST-C7,[16] and CMR7[15] methods require the *S*-spin nutation frequency ω_{nut}^S to be 7 times the sample spinning frequency, $\omega_{\mathrm{nut}}^S = 7\omega_r$. This is not usually a severe problem for samples containing only one type of spin, since nutation frequencies of around 120 kHz are routinely available.[27] However, the situation is more difficult in the context of biomo-

a)Electronic mail: mhl@physc.su.se

lecular NMR, where the *S*-spins usually take the form of introduced ^{13}C labels immersed in a pool of abundant protons (henceforth denoted *I*). It is necessary to decouple the *I*-spins from the *S*-spins at the same time as recoupling the *S*-spins with each other. Heteronuclear decoupling is usually achieved by applying a strong unmodulated rf field at the *I*-spin Larmor frequency, at the same time as the recoupling rf field on the *S*-spins. It has been found empirically that the *I*-spin nutation frequency must approach 3 times the *S*-spin nutation frequency in order to achieve good heteronuclear recoupling in this context, $\omega_{\rm nut}^I \gtrsim 3\omega_{\rm nut}^S$.[15] This is a restrictive condition, since most NMR probes do not tolerate very high rf fields on two irradiation channels at the same time. The need for good heteronuclear recoupling has so far restricted the biomolecular applications of C7 and its relatives to rather low spinning frequencies (typically around 6 kHz), which leads to a loss of sensitivity, mainly due to chemical shift anisotropy modulations during the signal acquisition.[34]

The rf field requirements of C7 may be reduced by employing fivefold symmetry instead of sevenfold symmetry. This introduces additional error terms which must be compensated by doubling the length of the sequence. The resulting cycle is called SPC-5 and has the matching condition $\omega_{\rm nut}^S = 5\omega_r$.[17]

Recently, we showed that the symmetry arguments leading to the original C7 sequence may be generalized.[35] A class of pulse sequences denoted CN_n^ν has been described, in which the symmetry-allowed terms in the average Hamiltonian are chosen according to simple theorems. The problem of heteronuclear decoupling in rotating solids was addressed using the CN_n^ν concept.[35]

In the current paper, the nature of CN_n^ν sequences is explored further. The CN_n^ν symmetry is identified as providing synchronized helical modulations of the space and the spin parts of the spin Hamiltonian. The labels *m* and ν indicate the *winding numbers* of the space and spin helices. We show that generalized helical symmetry admits solutions for homonuclear recoupling with lower rf field requirements than the original C7 sequences. We describe a new sequence, denoted $C14_4^5$, which has an rf field requirement of $\omega_{\rm nut}^S = 3.5\omega_r$, i.e., half of that required in the original C7 method. This allows application at fairly high spinning frequencies while still achieving good heteronuclear decoupling.

The pulse sequence $C14_4^5$ permits operation at high spinning frequencies but is not very well compensated for chemical shift perturbations. In order to further improve its performance we employ a supercycle scheme which combines high double-quantum efficiency with the compensation for chemical shifts. The supercycled sequence, called SC14, is roughly as broadband as previous recoupling schemes, while permitting application at higher spinning frequency.

Double-quantum recoupling is expected to be particularly useful in the spectroscopy of heavily labeled biomolecules, which are often easier and cheaper to synthesize than selectively labeled substances. Multidimensional spectroscopy will play an important role in spectral assignment, and in deriving multiple geometric constraints by simultaneous distance and angle estimations. Success of this approach will require a solid understanding of the dynamics of recoupled multiple-spin systems. In general, the effective recoupling Hamiltonian induces global spin dynamics which involve all recoupled spins at the same time. In this paper we investigate the dynamics of double-quantum excitation in a $^{13}C_3$ cluster. We obtain quantitative agreement between the amplitude development of experimental two-dimensional spectral peaks with analytical results, as well as with numerically exact simulations using the known molecular geometry. In addition we explore the theoretical phase properties of two-dimensional double-quantum spectra in multiple-spin recoupled systems and present approximate analytical expressions for individual peak amplitudes, as a function of the excitation and reconversion intervals. To demonstrate the practical utility of the new sequences, we show an experimental double-quantum spectrum of [U–^{13}C]–L-tyrosine, obtained at a spinning frequency of 20.000 kHz.

II. HELICAL RECOUPLING SEQUENCES

A. Synchronous helical modulations

The symbol CN_n^ν refers to a set of rotor synchronized rf pulse cycles, with the following properties: (i) Each rf cycle has a duration $\tau_{\rm C} = n\tau_r/N$, where $\tau_r = |2\pi/\omega_r|$ is the rotation period, and ω_r is the sample rotation frequency. This implies that *N* rf cycles are timed to coincide with *n* sample rotation periods. (ii) Each rf cycle is designed to provide no net evolution of the nuclear spin states, when only the rf field is taken into account. (iii) The rf phase of consecutive cycles differs by $2\pi\nu/N$. The phase of the *p*th cycle is therefore given by $\Phi_p = \Phi_0 + 2\pi\nu p/N$, with $p = 0,1,2,\ldots$. Here Φ_0 is the initial phase of the whole block.

The duration of an entire CN_n^ν sequence is denoted $T = N\tau_{\rm C}$. The symmetry numbers *n* and ν may be thought of as ''winding numbers'' of two helices, one representing the spatial sample rotation, and one representing the phase rotations of the rf fields. A complete sequence consists of *n* complete sample rotations and ν complete rf phase rotations. The sample rotation is continuous, while the pulse phase rotations are performed in *N* discrete steps. A pictorial representation of this concept is given for two different cases in Fig. 1.

In the general case, each element C may itself consist of pulses with different phase. However, in this paper, we assume that the rf field is only subject to amplitude modulation (or a π phase shift) within each cycle C.

B. Space-spin selection rules

Consider a set of $\mathcal{N}$ *S*-spins, denoted $S_1, S_2, \ldots, S_{\mathcal{N}}$, experiencing spin–spin interactions and chemical shift interactions as well as a rotor-synchronized rf pulse sequence with the symmetry CN_n^ν. The spin interaction terms are conveniently described in the interaction frame of the rf field. As described in Refs. 14, 15, and 35, the interaction frame Hamiltonian at time point *t* may be written

$$\tilde{H}(t) = \sum_{\Lambda,l,m,\lambda,\mu} \tilde{H}_{lm\lambda\mu}^{\Lambda}(t), \tag{1}$$

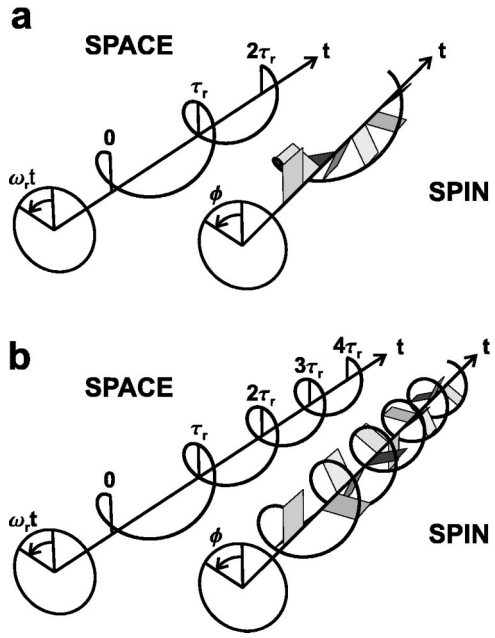

FIG. 1. Visualization of the synchronized helical modulations for two different CN_n^ν sequences. In each case the rotation of the space part of the Hamiltonian (sample rotation) is shown by a continuous spiral trajectory of the rotor phase, which completes n full revolutions. The trajectory of the spin part (rf phase) completes ν full revolutions in the same time, in N discrete steps. (a) Visualization of $C7_2^1$ symmetry. (b) Visualization of $C14_4^5$ symmetry.

where the symbol Λ represents the type of interaction (chemical shift, spin–spin coupling), and the quantum numbers l, m, λ, μ index the symmetry of the term with respect to rotations of the spin polarizations and with respect to spatial rotations of the sample. The term $\tilde{H}^\Lambda_{lm\lambda\mu}(t)$ transforms as an irreducible spherical tensor of rank l for spatial rotations and rank λ for spin rotations. The component indices m and μ have values $m=-l,-l+1,...,l$ for space and $\mu=-\lambda,-\lambda+1,...,\lambda$ for spin. For example, the direct dipole–dipole coupling between homonuclear spin pairs has ranks $l=2$, $\lambda=2$; the J-coupling between homonuclear spin pairs has ranks $l=0$, $\lambda=0$; the isotropic chemical shift has ranks $l=0$, $\lambda=1$; the chemical shift anisotropy and heteronuclear dipolar couplings have ranks $l=2$, $\lambda=1$. All components with $l=2$, $m=0$ vanish in the case of exact magic-angle spinning. Explicit expressions for the various terms may be found in Refs. 14 and 15.

As shown in Refs. 14, 15, and 35, the CN_n^ν symmetry of the pulse sequence imposes the following periodic symmetry on the interaction frame terms:

$$\tilde{H}^\Lambda_{lm\lambda\mu}(t+p\tau_C)=\tilde{H}^\Lambda_{lm\lambda\mu}(t)\exp\left\{i\frac{2\pi(mn-\mu\nu)p}{N}\right\}. \quad (2)$$

The results of the sequence may be analyzed using the Magnus expansion:[36,37]

$$\tilde{H}(t)=\bar{H}^{(1)}+\bar{H}^{(2)}+\bar{H}^{(3)}+\cdots, \quad (3)$$

where the first two orders[36] are given by

$$\bar{H}^{(1)}=T^{-1}\int_{t^0}^{t^0+T}dt\,\tilde{H}(t), \quad (4)$$

$$\bar{H}^{(2)}=(2iT)^{-1}\int_{t^0}^{t^0+T}dt'\int_{t^0}^{t'}dt[\tilde{H}(t'),\tilde{H}(t)], \quad (5)$$

if the sequence starts at time point t^0. The first order result for the effective Hamiltonian is

$$\bar{H}^{(1)}=\sum_{\Lambda,l,m,\lambda,\mu}\bar{H}^{\Lambda(1)}_{lm\lambda\mu}, \quad (6)$$

where

$$\bar{H}^{\Lambda(1)}_{lm\lambda\mu}=T^{-1}\int_{t^0}^{t^0+T}dt\,\tilde{H}^\Lambda_{lm\lambda\mu}(t). \quad (7)$$

As shown in Ref. 35, Eq. (2) leads to the following symmetry theorem:

$$\bar{H}^{\Lambda(1)}_{lm\lambda\mu}=0 \quad \text{if } mn-\mu\nu\neq N\times\text{integer}. \quad (8)$$

Similar theorems exist for the higher order Magnus terms.[35] The result Eq. (8) allows the design of sequences with desirable recoupling properties without calculation of the detailed structure of the cycle C, at least in the first stage of calculation.

The magnitude of the symmetry allowed terms depend on the details of the pulse sequence. In general, a symmetry allowed term has the form

$$\bar{H}^{\Lambda(1)}_{lm\lambda\mu}=\kappa_{lm\lambda\mu}[A^\Lambda_{lm}]^R\exp\{-im(\alpha^0_{RL}-\omega_r t^0)\}T^\Lambda_{\lambda\mu}, \quad (9)$$

where $[A^\Lambda_{lm}]^R$ is a space component of the interaction tensor Λ, written in the rotor-fixed frame, and α^0_{RL} denotes the initial rotor position. For sequences involving only π phase shifts, the scaling factor $\kappa_{lm\lambda\mu}$ of a symmetry allowed term with the quantum numbers (l,m,λ,μ) is given by

$$\kappa_{lm\lambda\mu}=i^\mu d^l_{m0}(\beta_{RL})\tau_C^{-1}\times\int_0^{\tau_C}dt\,d^\lambda_{\mu0}(-\beta_{\text{nut}}(t))\exp\{im\omega_r t\}, \quad (10)$$

where β_{RL} defines the angle between the rotor axis and the field, and the rf nutation angle is

$$\beta_{\text{nut}}(t)=\int_{t^0}^{t^0+t}dt'\,\omega_{\text{nut}}(t') \quad (11)$$

as described more fully in Ref. 35.

The consequences of Eq. (8) are conveniently explored using space-spin selection diagrams (SSS diagrams)[38] as shown in Figs. 2 and 3. These diagrams are similar to the coherence transfer pathway diagrams (CTP diagrams)[39] used in the design of phase cycling schemes. The resemblance to CTP diagrams is not coincidental: CTP diagrams help one visualize symmetry selection of terms under rotations of the spin polarizations around the field axis (coherence order). In a rotating sample exposed to an rf field, one must take into account the effect of macroscopic sample rotation, as well as spin rotations, and this is the task of the SSS diagrams shown in the current paper.

Figure 2 shows SSS diagrams for the $C7_2^1$ sequence. The plotted levels indicate the total value of $mn-\mu\nu$. The superposition of mn and $-\mu\nu$ is broken into two stages, so as to separate out the effects of spatial rotations and spin rotations. The ''barrier'' at the right-hand side of the diagrams

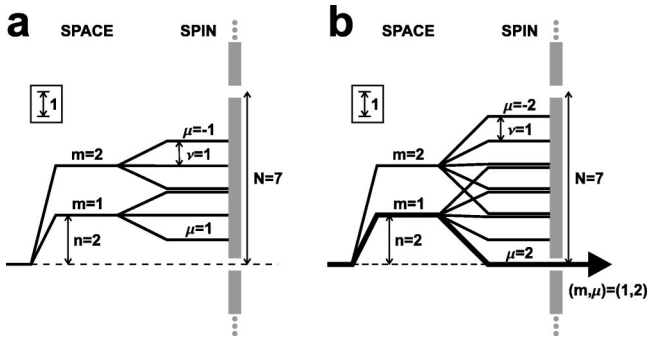

FIG. 2. Space-spin selection diagram (SSS diagram) for $C7_2^1$. (a) Suppression of all CSA modulation components. (b) Selection of a single 2Q dipole–dipole component, with quantum numbers $(m,\mu)=(1,2)$. The mirror image pathways stemming from $m=-1$, $m=-2$ have been suppressed for simplicity.

has holes separated by N units, which corresponds to the inequality in the symmetry theorem Eq. (8). Pathways which pass through a hole in the barrier indicate space-spin components which are symmetry allowed in the first order average Hamiltonian.

Figure 2(a) shows that all CSA components ($m=\{\pm1, \pm2\}$ and $\mu=\{0,\pm1\}$) are suppressed by $C7_2^1$ symmetry in the first order average Hamiltonian. Figure 2(b) shows that only homonuclear dipolar components with $(m,\mu)=(1,2)$ are symmetry allowed [and by implication, also $(m,\mu)=(-1, -2)$]. The selection of terms with $\mu=\pm2$ indicates double-quantum recoupling of the nuclear spin system. Furthermore, the fact that the $\mu=+2$ term is associated with only one spatial rotational component ($m=1$) is associated with a favorable orientation dependence of the double-quantum excitation.[14] One of the orientational Euler angles is ''phase-encoded,'' implying that the phase, but not the amplitude, of the recoupled double-quantum Hamiltonian depends on the value of this angle. This property is partly responsible for the high efficiency of C7 sequences in nonoriented samples.[14]

The symmetry properties of $C7_2^1$, as visualized in Fig. 2, are independent of the detailed structure of C. The optimal choice of C is dictated by other considerations, for example, the magnitude of the symmetry-allowed terms, the suppression of interference from isotropic chemical shifts, and the robustness of the sequence with respect to rf inhomogeneity. The cycles $C_0=(2\pi)_0(2\pi)_\pi$ and $C_0=(\pi/2)_0(2\pi)_\pi(3\pi/2)_0$ have both been exploited in the context of $C7_2^1$ symmetry.[14,16] Both cycles are internally compensated for rf inhomogeneity effects, and the latter choice gives an overall sequence which is particularly robust with respect to chemical shifts and rf inhomogeneity.[16]

The solution $N=7$, $n=2$, $\nu=1$ is far from unique. Table I shows some additional solutions for phase encoded double-quantum recoupling. The symmetry $C7_5^1$ has been pointed out before.[15,38] The symmetries $C7_1^3$, $C9_1^4$, $C11_1^5$, and $C13_1^6$ are particularly interesting, since they permit selective phase-encoded double-quantum recoupling within a single rotor period.

In addition, the interaction frame symmetry Eq. (2) may be generated by pulse sequences in which the rf fields do not obviously conform to the CN_n^ν pattern. This has been discussed briefly in the context of TPPM decoupling.[35] In a forthcoming paper, we show that this concept may be exploited to generate even more restrictive selection rules for the average Hamiltonian.[40]

TABLE I. A list of inequivalent CN_n^ν symmetries with $N\leqslant14$, $n\leqslant5$ and $0\leqslant\nu\leqslant N/2$, suitable for γ-encoded double-quantum recoupling. The symmetry-allowed terms with $m=\pm1$ and $\mu=\pm2$ are shown. All other terms with $m=\pm1,\pm2$ and $\mu=0,\pm1,\pm2$ are suppressed in the first order average Hamiltonian. Additional variants with similar properties for CN_n^ν are given by $CN_n^{ZN\pm\nu}$ where Z is an integer.

Sequence	(m,μ)		Sequence	(m,μ)	
$C7_1^3$	$(-1,2)$	$(1,-2)$	$C7_3^2$	$(-1,2)$	$(1,-2)$
$C9_1^4$	$(-1,2)$	$(1,-2)$	$C11_3^4$	$(-1,2)$	$(1,-2)$
$C11_1^5$	$(-1,2)$	$(1,-2)$	$C13_3^5$	$(-1,2)$	$(1,-2)$
$C13_1^6$	$(-1,2)$	$(1,-2)$			
			$C7_4^2$	$(-1,-2)$	$(1,2)$
$C7_2^1$	$(-1,-2)$	$(1,2)$	$C9_4^2$	$(-1,-2)$	$(1,2)$
$C8_2^1$	$(-1,-2)$	$(1,2)$	$C10_4^3$	$(-1,2)$	$(1,2)$
$C8_2^3$	$(-1,2)$	$(1,-2)$	$C11_4^2$	$(-1,-2)$	$(1,2)$
$C9_2^1$	$(-1,-2)$	$(1,2)$	$C13_4^2$	$(-1,-2)$	$(1,2)$
$C10_2^1$	$(-1,-2)$	$(1,2)$	$C14_4^5$	$(-1,2)$	$(1,-2)$
$C11_2^1$	$(-1,-2)$	$(1,2)$			
$C12_2^1$	$(-1,-2)$	$(1,2)$	$C7_5^1$	$(-1,2)$	$(1,-2)$
$C12_2^5$	$(-1,2)$	$(1,-2)$			
$C13_2^1$	$(-1,-2)$	$(1,2)$	$C9_5^2$	$(-1,2)$	$(1,-2)$
			$C11_5^3$	$(-1,2)$	$(1,-2)$
			$C13_5^4$	$(-1,2)$	$(1,-2)$

C. rf amplitude compensation

In this paper, we concentrate on the properties of the sequence $C14_4^5$, which has the SSS diagram shown in Fig. 3. The space-spin selection properties are identical to that of $C7_2^1$, except that the components $(m,\mu)=(-1,2)$ and $(1,-2)$ are selected instead of (1, 2) and $(-1, -2)$.

Although the SSS properties of $C7_2^1$ and $C14_4^5$ are essentially equivalent in the first order average Hamiltonian, the sequences differ in their robustness with respect to rf amplitude errors. The reason for this is illustrated in Fig. 4, which

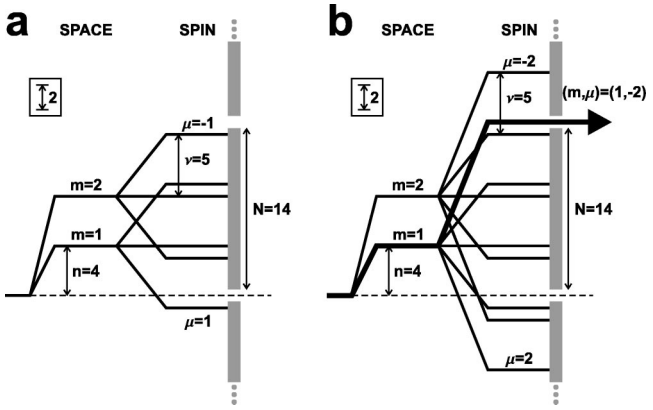

FIG. 3. Space-spin selection diagram (SSS diagram) for $C14_4^5$. (a) Suppression of all CSA modulation components. (b) Selection of a single 2Q dipole–dipole component, with quantum numbers $(m,\mu)=(1,-2)$. The vertical scale of this figure is one half that of Fig. 2. The mirror image pathways stemming from $m=-1$, $m=-2$ have been suppressed for simplicity.

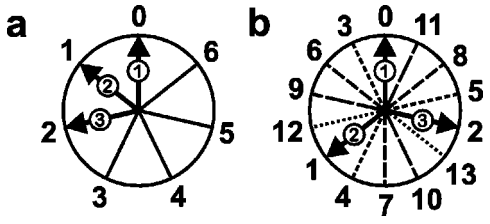

FIG. 4. (a) rf fields used in $C7_2^1$, denoted as vectors in the transverse plane. The numbers refer to the cycle index $q=0,1,...,6$. The first three elements of the sequence are denoted as bold vectors. (b) rf fields used in $C14_4^5$. The numbers refer to the cycle index $q=0,1,...,13$. The first three elements of the sequence are denoted as bold vectors. Consecutive phase values which combine to give good rf error compensation are drawn with the same line style.

shows the sequence of rf phases used in the two sequences. In Fig. 4(a) the sequence of rf fields in the transverse plane is illustrated for the case of $C7_2^1$. The phases are incremented between cycles in steps of $2\pi/7$. Suppose that each cycle rotates the spin polarizations through an angle slightly greater than 2π. In a first order approximation, the accumulated rotations cancel out after a full set of seven cycles. However, this cancellation is established very slowly, and in practice, only very small rotation errors are tolerated. It is therefore necessary to use the symmetry $C7_2^1$ in combination with a cycle which is *internally* compensated for rf amplitude errors. The cycles $C_0=(2\pi)_0(2\pi)_\pi$ and $C_0=(\pi/2)_0(2\pi)_\pi(3\pi/2)_0$ fulfill this condition, at the expense of requiring an rf field which is twice as large as for the simplest possible sequence $C_0=(2\pi)_0$, which is uncompensated for rf field amplitude errors.

The situation for $C14_4^5$ is different, as shown in Fig. 4(b). Here the step in phase between consecutive cycles is $10\pi/14\cong 129°$. Since this is close to the angle $2\pi/3=120°$, each group of three consecutive cycles is well compensated for rotation errors. This may be visualized by adding together the bold vectors in Fig. 4(b). The symmetry $C14_4^5$ is therefore intrinsically compensated for rf amplitude errors, and internal compensation of the cycle C may be dispensed with. It is feasible to use the simplest possible cycle $C_0=(2\pi)_0$, allowing a reduction of the required rf field by a factor of 2, for a given spinning frequency, compared to $C7_2^1$ sequences employing cycles of the form $C_0=(2\pi)_0(2\pi)_\pi$ or $C_0=(\pi/2)_0(2\pi)_\pi(3\pi/2)_0$.

This compensation mechanism is independent of the sign of ν. However, in practice sequences with opposite signs of ν have slightly different performances, because the chemical shift anisotropy interactions have a defined sign. This is illustrated by the simulations in Fig. 5(a), which show the calculated double-quantum filtered efficiency as a function of rf irradiation frequency, for parameters corresponding to $[^{13}C_2,^{15}N]$-glycine at a field of 9.4 T.[41] In most of the experimental results shown below, we employ $C14_4^{-5}$ instead of $C14_4^5$. In all experimental implementations we take into account the sense of the Larmor frequency as well as the radio frequency mixing scheme, as described in Refs. 42 and 43.

Experimental evidence of the rf compensation mechanism of $C14_4^{-5}$ is shown in Fig. 6, which shows experimental results for $[^{13}C_2,^{15}N]$-glycine, obtained at a spinning frequency of $\omega_r/2\pi=11.000$ kHz. The figure shows integrals of double-quantum-filtered spectra as a function of rf field amplitude for the sequences $C7_2^1$ and $C14_4^{-5}$. Both sequences use an uncompensated elemental cycle $C_0=(2\pi)_0$. The $C7_2^1$ symmetry performs rather poorly in this case. The improved robustness of the $C14_4^{-5}$ cycle is visually obvious.

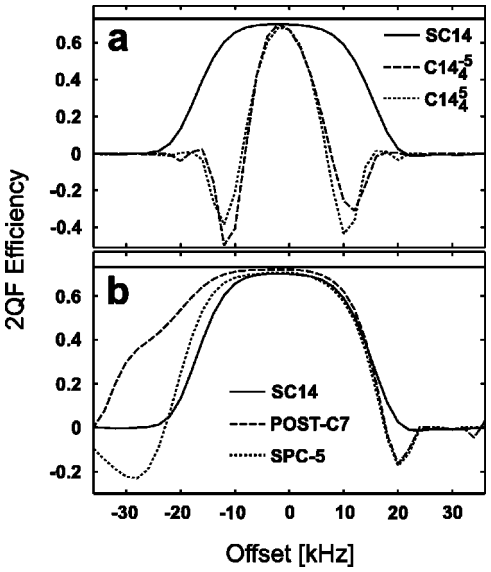

FIG. 5. Simulated double-quantum filtered efficiencies for (a) SC14, $C14_4^{-5}$, $C14_4^5$; (b) SC14, POST-C7, SPC-5. The simulations are done for the parameters of $[^{13}C_2]$-glycine at a field of $B_0=9.4$ T (Ref. 41). Powder averaging was performed using 538 orientations Ω_{MR}, chosen according to the ZCW scheme (Ref. 62). In all cases the rf amplitude is given by $\omega_{\mathrm{nut}}^S/2\pi=70.070$ kHz. The spinning frequency, the excitation and reconversion intervals are given by SC14, $C14_4^5$, $C14_4^{-5}$: $\omega_r/2\pi=20.020$ kHz, $\tau_E=\tau_R=599.4\ \mu$s; POST-C7: $\omega_r/2\pi=10.010$ kHz, $\tau_E=\tau_R=599.4\ \mu$s; SPC-5: $\omega_r/2\pi=14.014$ kHz, $\tau_E=\tau_R=713.6\ \mu$s. The theoretical maximum of 73% is indicated by a solid line.

It should be noted that the sequence $C14_4^{-5}$ may be derived from two consecutive $C7_2^1$ sequences, by adding π to the phase of odd numbered C elements, and continuing the pattern through four rotor periods.

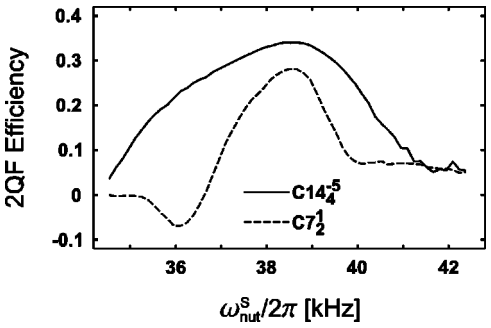

FIG. 6. Experimental measurements of double-quantum filtered efficiency for $C7_2^1$ and $C14_4^{-5}$ sequences, obtained on $[^{13}C_2,^{15}N]$-glycine (98% ^{13}C, 96–99 % ^{15}N), at a field of $B_0=4.7$ T and a spinning frequency of $\omega_r/2\pi=11.000$ kHz using a Chemagnetics-Infinity-200 spectrometer, and a cross-polarization contact time of 1.4 ms. The sample was purchased from Cambridge Isotope Laboratories and used without further purification. The excitation and reconversion intervals were both $\tau_E=\tau_R=519.4\ \mu$s. Continuous wave decoupling was applied with the proton nutation frequency 122 kHz during CN_n^ν, and 86 kHz during acquisition. An elemental cycle $C_0=(2\pi)_0$ was used in both cases. The ^{13}C nutation frequency is varied along the horizontal axis. The $C14_4^{-5}$ sequence is clearly more robust with respect to rf amplitude errors.

As shown in Table I, there are many other feasible solutions for the symmetry numbers N, μ, and ν. For example, the symmetry $C7_5^1$ may be used in conjunction with the cycle $C_0=(2\pi)_0(2\pi)_{2\pi/3}(2\pi)_{4\pi/3}$ to provide a sequence with good rf amplitude compensation and low rf power requirements: $\omega_{\mathrm{nut}}^S=4.2\omega_r$.[38] The cycles $C_0=(2\pi)_0(2\pi)_\pi$ and $C_0=(\pi/2)_0(2\pi)_\pi(3\pi/2)_0$ are poor choices in this context, because they lead to very small magnitudes for the recoupled 2Q term.[15] The cycle $C_0=(2\pi)_0(2\pi)_{2\pi/3}(2\pi)_{4\pi/3}$ does not suffer from this defect and leads to a $C7_5^1$ sequence which is almost as efficient as the $C14_4^{-5}$ sequence based on $C_0=(2\pi)_0$. Table I presumably contains many other solutions with favorable properties, some of which may allow operation at even higher spinning frequency than $C14_4^{-5}$.

D. Supercycle construction

The sequence $C14_4^{-5}$ with $C_0=(2\pi)_0$ has fairly good rf error compensation but is not well compensated with respect to resonance offset effects and chemical shift anisotropies. This is illustrated in Fig. 5(a). We have constructed supercycles of $C14_4^{-5}$ which have an acceptable chemical shift compensation. One example is the supercycle

$$\mathrm{SC14}=\mathrm{C14}_4^5\cdot[\Pi_0^{-1}\cdot\mathrm{C14}_4^{-5}\cdot\Pi_0]_{\pi/7}\cdot[\mathrm{C14}_4^5]_\pi\cdot[\Pi_0^{-1}\cdot\mathrm{C14}_4^{-5}\cdot\Pi_0]_{8\pi/7},$$

where the notation Π_0 indicates the insertion of a π pulse element with phase $\phi=0$ and Π_0^{-1} indicates the deletion of a π-pulse element. The notation $[\cdots]_\phi$ indicates an overall phase shift of the bracketed sequence by ϕ. The sequence $[\Pi_0^{-1}\cdot\mathrm{C14}_4^{-5}\cdot\Pi_0]_{\pi/7}$ is therefore a phase-shifted cyclic permutation of the $C14_4^{-5}$ sequence. The full SC14 sequence may be written as follows:

$$\begin{array}{cccccccc}
360_0 & 360_{128.57} & 360_{257.14} & 360_{25.71} & 360_{154.29} & 360_{282.86} & 360_{51.43} & \\
360_{180} & 360_{308.57} & 360_{77.14} & 360_{205.71} & 360_{334.29} & 360_{102.86} & 360_{231.43} & \\
180_{25.71} & 360_{257.14} & 360_{128.57} & 360_0 & 360_{231.43} & 360_{102.86} & 360_{334.29} & \\
360_{205.71} & 360_{77.14} & 360_{308.57} & 360_{180} & 360_{51.43} & 360_{282.86} & 360_{154.29} & 180_{25.71} \\
360_{180} & 360_{308.57} & 360_{77.14} & 360_{205.71} & 360_{334.29} & 360_{102.86} & 360_{231.43} & \\
360_0 & 360_{128.57} & 360_{257.14} & 360_{25.71} & 360_{154.29} & 360_{282.86} & 360_{51.43} & \\
180_{205.71} & 360_{77.14} & 360_{308.57} & 360_{180} & 360_{51.43} & 360_{282.86} & 360_{154.29} & \\
360_{25.71} & 360_{257.14} & 360_{128.57} & 360_0 & 360_{231.43} & 360_{102.86} & 360_{334.29} & 180_{205.71}
\end{array} \tag{12}$$

where all flip angles and phases are specified in degrees. The complete sequence spans 16 rotor periods. The theoretical principles of this supercycle are discussed in Appendix A.

The performance of SC14 with respect to resonance offset is illustrated in Fig. 5 (solid lines). Figure 5(b) shows that the maximum double-quantum efficiency and offset performance are comparable to those of POST-C7 and SPC-5 (dashed and dotted lines) under these conditions. Note that all simulations are performed at the same rf field strength, corresponding to a nutation frequency of $\omega_{\mathrm{nut}}^S/2\pi=70.070$ kHz. However, the sample spinning frequencies are different in the three cases, corresponding to 10.010 kHz for POST-C7, 14.014 kHz for SPC-5, and 20.020 kHz for SC14. Figure 5(b) illustrates the point that SC14 permits double-quantum excitation at higher spinning frequencies than previous pulse sequences, in the case that the rf field strength is limited by probe performance and heteronuclear decoupling requirements. In multiply labeled spin systems, it is generally desirable to rotate the sample as fast as possible, in order to achieve optimal sensitivity and resolution.[44]

Although SC14 performs well at high spinning frequencies, simulations indicate that it performs poorly at low spinning frequencies. Sequences such as POST-C7 should be used in this regime.

III. DOUBLE-QUANTUM SPECTROSCOPY OF MULTIPLE-SPIN SYSTEMS

A. Pulse sequence

Double-quantum spectroscopy of ^{13}C-labeled organic solids at high MAS spinning frequencies may be performed using the radio frequency (rf) pulse sequence shown in Fig. 7. The row marked I denotes the rf fields at the Larmor frequency of the abundant protons, while S denotes the rf fields applied at the ^{13}C Larmor frequency. The sequence starts with ramped cross polarization to enhance the S-spin magnetization.[45] The following $\pi/2$-pulse converts the transverse magnetization into longitudinal S-spin magnetization. The ramped cross-polarization field and the $\pi/2$ pulse have the phases Φ_{prep} and $\Phi_{\mathrm{prep}}-\pi/2$ respectively, where Φ_{prep} is the overall rf phase of the preparation interval.

The $\pi/2$-pulse is followed by a 2Q-excitation pulse sequence of duration τ_E. The 2Q-excitation sequence converts the S-spin longitudinal magnetization into (±2)-quantum coherence. The double-quantum excitation sequence starts at the time point t_E^0 and terminates at time point $t_E^1=t_E^0+\tau_E$.

In the following discussion, we assume that a $C14_4^{-5}$ sequence is used for the double-quantum excitation and reconversion as shown in Fig. 7. The SC14 supercycle is demonstrated later on in this paper.

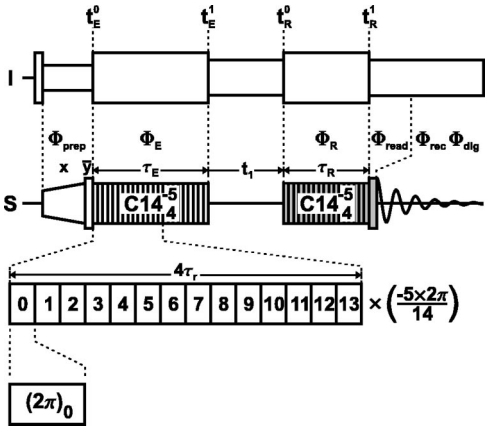

FIG. 7. Radio frequency pulse sequence for double-quantum 2D spectroscopy using $C14_4^{-5}$. The phases Φ_{prep}, Φ_E, Φ_R, Φ_{read} refer to overall rf phases of the pulse sequence blocks. The rf receiver phase during signal detection is denoted Φ_{rec} and the post-digitization phase by Φ_{dig}.

The excitation part of the sequence consists of q_E cycles, corresponding to an excitation interval of $\tau_E = q_E \tau_C$. The overall phase of the excitation block denoted is Φ_E so that the rf cycles have phases Φ_E, $\Phi_E - 10\pi/14$, $\Phi_E - 20\pi/14$, etc. Note that the number of cycles q_E is not restricted to be a multiple of 14.

The excited double-quantum coherences are allowed to evolve for an interval t_1, and are reconverted into longitudinal S-spin magnetization by applying another q_R cycles of $C14_4^{-5}$ irradiation. The reconversion block has duration $\tau_R = q_R \tau_C$ and an overall phase Φ_R, so that the rf phases are given by Φ_R, $\Phi_R - 10\pi/14$, $\Phi_R - 20\pi/14$, etc. The longitudinal magnetization created by the second $C14_4^{-5}$ sequence is converted into observable magnetization by a $\pi/2$ read pulse, whose phase is denoted Φ_{read}.

The complex NMR signal is detected in the subsequent period using a rf receiver phase Φ_{rec} and post-digitization phase shift Φ_{dig}.[42] A two-dimensional data matrix $s(t_1, t_2)$ is compiled by acquiring a set of transients with incrementation of the interval t_1.

The specification of the rf phases is quite complicated because of (i) phase cycling in order to select signals passing through (± 2)-quantum coherence in the t_1 interval; (ii) the special phase-timing relationships which are required for CN_n^ν sequences in the case that an integer number of full cycles is not completed; (iii) the time-proportional phase incrementation (TPPI) procedure for separating the (± 2)-quantum signals.[39]

The phases Φ_{prep}, Φ_E, Φ_R, Φ_{read}, Φ_{rec}, and Φ_{dig} are conveniently specified in terms of the transient counter m_2 and the evolution increment counter m_1. The counter $m_2 = 0,1,...,15$ is incremented on every acquired transient, while m_1 is incremented between different values of t_1. The phase specifications are

$$\Phi_{\mathrm{prep}} = \Phi_E = \frac{\pi}{4} m_1,$$

$$\Phi_R(t_1) = \Phi_R^0(t_1) + \frac{\pi}{2} m_2,$$

$$\Phi_{\mathrm{read}} = \frac{\pi}{2} + \frac{\pi}{2} m_2 + \frac{\pi}{2} \mathrm{floor}\left(\frac{m_2}{4}\right), \tag{13}$$

$$\Phi_{\mathrm{rec}} = 0,$$

$$\Phi_{\mathrm{dig}} = -\Phi_{\mathrm{rec}} - 2(\Phi_R(t_1) - \Phi_R^0(t_1)) + \Phi_{\mathrm{read}} - \frac{\pi}{2},$$

where the function floor(x) returns the largest integer not greater than x. The base reconversion phase for the phase $\Phi_R^0(\tau_1)$ is given by

$$\Phi_R^0(\tau_1) = \frac{\pi}{2} + \frac{1}{2}\omega_r(t_R^0 - t_E^0), \tag{14}$$

where t_E^0 and t_R^0 are the time points marking the start of the two $C14_4^{-5}$ sequences. The interval between these time points depends on the evolution interval t_1 according to

$$t_R^0 - t_E^0 = \tau_E + t_1 \tag{15}$$

as may be seen in Fig. 7. The link Eq. (14) between the pulse sequence phases and timings allows a completely general incrementation of the evolution interval.[41,46] A more restricted version of this result was given earlier by Hong.[47] In practice a more specific form of Eq. (14) has proven to be useful, which for $C14_4^{-5}$ is given by[46]

$$\Phi_R^0(t_1) = \frac{\pi}{2} - \frac{10\pi}{4} q_E + \frac{1}{2}\omega_r t_1. \tag{16}$$

The data matrix $s(t_1, t_2)$ is subjected to a complex Fourier transform in the t_2 dimension, and a cosine Fourier transform in the t_1 dimension, in order to obtain the 2D spectrum $S(\omega_1, \omega_2)$. Under suitable conditions, the 2D spectrum contains pure absorption double-quantum peaks as discussed in the next section.

B. Average Hamiltonian and pulse sequence propagators

Although C7-like pulse sequences have been used for two-dimensional double-quantum spectroscopy,[27,47] an explicit theory of this experiment has not been given so far. In the following sections, we develop this theory, concentrating particularly on the amplitudes and phases of the two-dimensional peaks.

Suppose that a double-quantum recoupling sequence is applied to a set of $\mathcal{N}$ coupled S-spins, denoted $S_1, S_2, \ldots, S_{\mathcal{N}}$. The sequence starts at time point t^0, with an overall rf phase Φ^0. The time-independent average Hamiltonian under the rf pulse sequence is given by

$$\bar{H}^{(1)} = \sum_{j<k} \bar{H}_{jk}^{(1)}, \tag{17}$$

where the sum is taken over all spin pairs. For $C7_2^1$, $C14_4^{-5}$ and many other double-quantum recoupling sequences,[13,15,17] the average Hamiltonian $\bar{H}_{jk}^{(1)}$ for a single molecular orientation has the following form:

$$\bar{H}_{jk}^{(1)} = \omega_{jk}^* \tfrac{1}{2} S_j^+ S_k^+ + \omega_{jk} \tfrac{1}{2} S_j^- S_k^- + 2\pi J_{jk} \mathbf{S}_j \cdot \mathbf{S}_k, \tag{18}$$

where J_{jk} is the J-coupling between spins S_j and S_k, ω_{jk} the recoupled through-space dipolar interaction and the asterisk

denotes the complex conjugate. For the specific case of $C14_4^{-5}$, the recoupled double-quantum dipolar interaction depends on the molecular orientation, the time point t^0, and the rf phase Φ^0 according to

$$\omega_{jk}(\Omega_{MR},t^0,\Phi^0)=\sqrt{6}b_{jk}\kappa e^{i(-\omega_r t^0+\alpha_{RL}^0+\gamma_{MR}+2\Phi^0)} \times\sum_{m=-2}^{2} d_{0m}^{(2)}(\beta_{PM}^{jk})d_{m-1}^{(2)}(\beta_{MR}) \times e^{-im(\gamma_{PM}^{jk}+\alpha_{MR})}, \tag{19}$$

where $d_{nm}^{(2)}$ is a reduced Wigner element[48] and κ corresponds to κ_{2-12-2} in Eq. (10). The Euler angles $\Omega_{PM}^{jk}=\{\alpha_{PM}^{jk},\beta_{PM}^{jk},\gamma_{PM}^{jk}\}$ describe the transformation of each dipole–dipole coupling from its principal axis to a molecule fixed frame. The Euler angles $\Omega_{MR}=\{\alpha_{MR},\beta_{MR},\gamma_{MR}\}$ relate the molecular fixed frame to a frame fixed on the rotor. These angles are random variables in a powder. The through space dipolar coupling between two spins j and k is given by

$$b_{jk}=-\frac{\mu_0}{4\pi}\frac{\gamma_j\gamma_k\hbar}{r_{jk}^3}, \tag{20}$$

where r_{jk} is the spin–spin internuclear distance. The factor

$$\kappa=\frac{343(i-e^{-i(\pi/14)})}{768\sqrt{2}\pi} \tag{21}$$

represents the scaling factor of the homonuclear recoupling sequence. The $C14_4^{-5}$ sequence with $C_0=(2\pi)_0$ has a scaling factor $|\kappa|\cong 0.157$. This is slightly higher than that obtained for $C7_2^1$ with $C_0=(2\pi)_0(2\pi)_\pi$ (Ref. 14) or $C_0=(\pi/2)_0(2\pi)_\pi(3\pi/2)_0$,[16] which both have a scaling factor $|\kappa|\cong 0.155$. The definition of the scaling factor used here, Eq. (10) differs from that given in Ref. 16 by a factor of 2/3.

When a recoupling sequence is applied with overall rf phase Φ^0 and duration τ, starting from time point t^0, and ending at time point t^1, the corresponding propagation superoperator is

$$\hat{V}(t^1,t^0,\Phi^0)=\exp\{-i\hat{\bar{H}}^{\mathrm{comm}}(t^0,\Phi^0)\tau\}, \tag{22}$$

where $\hat{\bar{H}}^{\mathrm{comm}}$ denotes the commutation superoperator[49] of the average Hamiltonian $\bar{H}^{(1)}$. We assume that the average Hamiltonian is independent of the time interval τ. This assumption is tested later by comparison with accurate simulations.

From Eq. (19) the form of the propagation superoperator is

$$\hat{V}(t^1,t^0,\Phi^0)=\hat{R}_z(\Phi^0-\tfrac{1}{2}\omega_r t^0)\hat{V}^0(\tau)\hat{R}_z(-\Phi^0+\tfrac{1}{2}\omega_r t^0), \tag{23}$$

where $\hat{R}_z(\phi)$ is the rotation superoperator[49]

$$\hat{R}_z(\phi)=\exp\{-i\phi\hat{S}_z^{\mathrm{comm}}\} \tag{24}$$

and $\hat{S}_z^{\mathrm{comm}}$ is the superoperator for commutation with the total spin angular momentum along the z axis. $\hat{V}^0(\tau)$ is the propagator for a $C14_4^{-5}$ sequence with duration τ, starting at time point $t=0$ and an overall phase $\Phi^0=0$:

$$\hat{V}^0(\tau)=\exp\{-i\hat{\bar{H}}^{\mathrm{comm}}(0,0)\tau\}. \tag{25}$$

Equation (23) indicates an explicit relationship between the effective phase of the propagation superoperator and the pulse sequence timings. In the experiments, this link is exploited to allow arbitrary incrementation of the evolution interval t_1.

C. Double-quantum spectra

Consider the pulse sequence in Fig. 7. The (-1)-quantum coherence generated by the last $\pi/2$ pulse is detected at time point t_2, using pulse sequences with different evolution intervals t_1. The complex 2D signal amplitude may be written

$$s(t_1,t_2)=i(S_z|S_z)^{-1}(S^-|\hat{U}_0(t_2,0)\hat{R}_x\left(\frac{\pi}{2}\right) \times\hat{V}_R\hat{U}_0(t_R^0,t_E^1)\hat{V}_E|S_z), \tag{26}$$

where $\hat{U}_0(t_b,t_a)$ expresses free propagation in the absence of rf fields, from time point t_a to time point t_b. $\hat{V}_E$ and $\hat{V}_R$ are shorthand notations for $\hat{V}_E=\hat{V}(t_E^1,t_E^0,\Phi_E)$ and $\hat{V}_R=\hat{V}(t_R^1,t_R^0,\Phi_R)$. The factor i takes into account quadrature signal detection.[42] In addition a normalization factor $(S_z|S_z)^{-1}$ has been included. The (-1)-quantum operator may be written as a superposition of terms from individual spins:

$$(S^-|=\sum_l (S_l^-|=\sum_l (S_{lx}-iS_{ly}|. \tag{27}$$

If the experiment is performed far from rotational resonance,[1–6] and CSA modulations are ignored, the evolution of the individual (-1)-quantum coherences may be written as

$$(S_l^-|\hat{U}_0(t_2,0)\cong\exp\{(i\omega_l^{\mathrm{iso}}-\lambda_l)t_2\}(S_l^-|, \tag{28}$$

where ω_l^{iso} is the isotropic chemical shift of spins S_l, and λ_l is the coherence decay constant. The result of the final $\pi/2$ pulse may be written

$$(S_l^-|\hat{R}_x\left(\frac{\pi}{2}\right)=(S_{lx}+iS_{lz}| \tag{29}$$

which leads to the following expressions for the 2D signal amplitude, neglecting CSA and rotational resonance effects:

$$s(t_1,t_2)\cong(S_z|S_z)^{-1}\sum_l (-iS_{lx}+S_{lz}|\hat{V}_R\hat{U}_0(t_1)\hat{V}_E|S_z) \times\exp\{(i\omega_l^{\mathrm{iso}}-\lambda_l)t_2\}. \tag{30}$$

The evolution propagator $\hat{U}_0(t_b,t_a)$ has been written as $\hat{U}_0(t_1)$, for the sake of brevity. Since the Hamiltonian in the absence of an rf field commutes with S_z, the central propagator may be written as

$$\hat{V}_R\hat{U}_0(t_1)\hat{V}_E=\hat{R}_z(\Phi_R-\tfrac{1}{2}\omega_r t_R^0)\hat{V}_R^0\hat{R}_z(-\Phi_R+\Phi_E+\tfrac{1}{2}\omega_r(t_R^0-t_E^0))\hat{U}_0(t_1)\hat{V}_E^0\hat{R}_z(-\Phi_E+\tfrac{1}{2}\omega_r t_E^0). \tag{31}$$

Using the relationship between the pulse sequence phases and timings [Eq. (14)], and taking into account the phase cycling, which selects double-quantum coherences during the evolution interval t_1 as well as z-magnetization at time point t_R^1, we get

$$\begin{aligned}\overline{s}(t_1,t_2) = &-(S_z|S_z)^{-1}\\ &\times\sum_l (S_{lz}|\hat{V}_R^0\hat{P}^{(2)}\hat{U}_0(t_1)\hat{V}_E^0|S_z)\\ &\times\exp\{(i\omega_l^{\rm iso}-\lambda_l)t_2\},\end{aligned} \tag{32}$$

where the overbar denotes the phase-cycled signal amplitude. The terms $\hat{V}_E^0$ and $\hat{V}_R^0$ are abbreviations for $\hat{V}^0(\tau_E)$ and $\hat{V}^0(\tau_R)$, respectively. The term $\hat{P}^{(2)}$ represents a projection superoperator for (± 2)-quantum coherences, which may be written in terms of the individual spin operators as follows:

$$\hat{P}^{(2)} = \hat{P}^{(+2)} + \hat{P}^{(-2)} \tag{33}$$

with

$$\begin{aligned}\hat{P}^{(+2)} &= \sum_{j<k}\frac{|S_j^+S_k^+)(S_j^+S_k^+|}{(S_j^+S_k^+|S_j^+S_k^+)},\\ \hat{P}^{(-2)} &= \sum_{j<k}\frac{|S_j^-S_k^-)(S_j^-S_k^-|}{(S_j^-S_k^-|S_j^-S_k^-)}.\end{aligned} \tag{34}$$

The sum is to be taken over all spin pairs and $(S_j^+S_k^+|S_j^+S_k^+) = (S_j^+S_k^+|S_j^+S_k^+) = 2^{\mathcal{N}-2}$. For simplicity, we have ignored contributions to the projection superoperator corresponding to double-quantum coherences involving more than two spins. There is no contribution from these terms in the case of two and three spin systems in general and in the case of a multiple-spin system for short time intervals τ_E and τ_R.

If rotational resonance effects and CSA modulations are ignored, the evolution of the individual (± 2)-quantum coherences has a simple form:

$$\begin{aligned}\hat{U}_0(t_1)|S_j^+S_k^+) &\cong |S_j^+S_k^+)\exp\{-i(\omega_j^{\rm iso}+\omega_k^{\rm iso})t_1-\lambda_{jk}t_1\},\\ \hat{U}_0(t_1)|S_j^-S_k^-) &\cong |S_j^-S_k^-)\exp\{+i(\omega_j^{\rm iso}+\omega_k^{\rm iso})t_1-\lambda_{jk}t_1\},\end{aligned} \tag{35}$$

where λ_{jk} is a double-quantum decay rate constant.

These expressions may be combined to obtain the phase-cycled 2D spectral amplitudes:

$$\overline{s}(t_1,t_2) \cong \sum_{j<k}\sum_l (s_{jk\to l}^{(+2)}(t_1,t_2) + s_{jk\to l}^{(-2)}(t_1,t_2)), \tag{36}$$

where

$$\begin{aligned}s_{jk\to l}^{(+2)}(t_1,t_2) &= a_{jk\to l}^{(+2)}\exp\{-i(\omega_j^{\rm iso}+\omega_k^{\rm iso})t_1 + i\omega_l^{\rm iso}t_2\\ &\quad -\lambda_{jk}t_1-\lambda_l t_2\},\\ s_{jk\to l}^{(-2)}(t_1,t_2) &= a_{jk\to l}^{(-2)}\exp\{+i(\omega_j^{\rm iso}+\omega_k^{\rm iso})t_1 + i\omega_l^{\rm iso}t_2\\ &\quad -\lambda_{jk}t_1-\lambda_l t_2\},\end{aligned} \tag{37}$$

and the 2D signal amplitudes (for a single molecular orientation) are

$$\begin{aligned}a_{jk\to l}^{(+2)}(\tau_E,\tau_R) &= -\mathfrak{N}\sum_m (S_{lz}|\hat{V}_R^0|S_j^+S_k^+)(S_j^+S_k^+|\hat{V}_E^0|S_{mz}),\\ a_{jk\to l}^{(-2)}(\tau_E,\tau_R) &= -\mathfrak{N}\sum_m (S_{lz}|\hat{V}_R^0|S_j^-S_k^-)(S_j^-S_k^-|\hat{V}_E^0|S_{mz}).\end{aligned} \tag{38}$$

The normalization factor $\mathfrak{N}$ is given by

$$\begin{aligned}\mathfrak{N} &= (S_j^+S_k^+|S_j^+S_k^+)^{-1}(S_z|S_z)^{-1}\\ &= (S_j^-S_k^-|S_j^-S_k^-)^{-1}(S_z|S_z)^{-1} = (\mathcal{N}2^{2\mathcal{N}-4})^{-1}.\end{aligned} \tag{39}$$

The term $a_{jk\to l}^{(+2)}$ represents the complex amplitude of the 2D spectral peak at the frequency coordinates $(\omega_1,\omega_2) = (-\omega_j^{\rm iso}-\omega_k^{\rm iso},\omega_l^{\rm iso})$. The term $a_{jk\to l}^{(-2)}$ represents the complex amplitude of the 2D spectral peak at the frequency coordinates $(\omega_1,\omega_2) = (\omega_j^{\rm iso}+\omega_k^{\rm iso},\omega_l^{\rm iso})$. The amplitudes depend on the orientation Ω_{MR} through Eq. (19). In a powder, the orientational average is observed:

$$\begin{aligned}\langle a_{jk\to l}^{(\pm 2)}\rangle_{\Omega_{MR}} = &\frac{1}{8\pi^2}\int_0^{2\pi}d\alpha_{MR}\int_0^{\pi}d\beta_{MR}\sin\beta_{MR}\\ &\times\int_0^{2\pi}d\gamma_{MR}\,a_{jk\to l}^{(\pm 2)}(\Omega_{MR}).\end{aligned} \tag{40}$$

The 2D spectral peaks fall into two classes: (i) Peaks of the form $(jk\to j)$ which represent transfer of double-quantum coherence between spins S_j and S_k into single-quantum coherence of a spin within the same pair. These peaks here referred to as *direct* double-quantum peaks. (ii) peaks of the form $(jk\to l)$, which represent transfer of double-quantum coherences between spins S_j and S_k into single-quantum coherence of a third spin S_l. These peaks are referred to as *indirect* double-quantum peaks.

D. Spectral amplitudes

The theoretical expressions Eq. (38) may be used to investigate the dependence of the 2D peak amplitudes on the excitation and reconversion intervals τ_E and τ_R. As shown in Appendix B, the Liouvillian matrix elements are related through

$$\begin{aligned}(S_{lz}|\hat{V}^0(\tau)|S_j^+S_k^+) &= (S_{lz}|\hat{V}^0(\tau)|S_j^-S_k^-)^*,\\ (S_j^+S_k^+|\hat{V}^0(\tau)|S_{lz}) &= (S_j^-S_k^-|\hat{V}^0(\tau)|S_{lz})^*.\end{aligned} \tag{41}$$

The (± 2)-quantum spectral amplitudes are therefore complex conjugates of each other:

$$a_{jk\to l}^{(-2)} = (a_{jk\to l}^{(+2)})^*. \tag{42}$$

This relationship is not sufficient to prove that 2D spectral peaks are pure absorption, after cosine transform in the t_1 dimension. As discussed in standard texts,[39] pure absorption spectra are obtained only if the amplitudes for the (± 2)-quantum pathways are *real*, as well as being equal.

It is useful to expand the terms in Eq. (38) with respect to the pulse sequence excitation and reconversion intervals τ_E and τ_R, using

$$(S_j^+ S_k^+|\hat{V}^0(\tau)|S_{lz}) = \mathrm{Tr}\{S_j^- S_k^- (S_{lz} + i\tau[\overline{H}^{(1)}, S_{lz}] + \frac{(i\tau)^2}{2!}[\overline{H}^{(1)}, [\overline{H}^{(1)}, S_{lz}]] + \cdots)\}. \tag{43}$$

Some labor is saved by using the symmetry relationship

$$(S_{lz}|\hat{V}^0(\tau)|S_j^{\pm} S_k^{\pm}) = -(S_j^{\pm} S_k^{\pm}|\hat{V}^0(\tau)|S_{lz})^* \tag{44}$$

which applies if J couplings are ignored, as proved in Appendix B. If the expansions are carried out to a total order of 4 for the τ_E and τ_R intervals, we get the following expressions for the direct double-quantum peaks, for a single molecular orientation:

$$a_{jk\to j}^{(+2)}(\tau_E, \tau_R) \cong \frac{1}{\mathcal{N}}\left\{\frac{1}{2}|\omega_{jk}|^2 \tau_E \tau_R - \frac{1}{12}|\omega_{jk}|^2\left(\sum_{l\neq j}|\omega_{jl}|^2 + \sum_{l\neq(j,k)}|\omega_{kl}|^2\right)\tau_E^3 \tau_R - \frac{1}{48}|\omega_{jk}|^2\left(4\sum_{l\neq j}|\omega_{jl}|^2 + \sum_{l\neq(j,k)}|\omega_{kl}|^2\right)\tau_E \tau_R^3 + \cdots\right\}. \tag{45}$$

The sum $\Sigma_{l\neq j}$ implies a sum over all values of l not equal to j, while the sum $\Sigma_{l\neq(j,k)}$ implies a sum over all values of l not equal to either j or k. For the indirect double-quantum peaks we get for a single molecular orientation

$$a_{jk\to l}^{(+2)}(\tau_E, \tau_R) \cong \frac{1}{\mathcal{N}}\left\{-\frac{1}{16}|\omega_{jk}|^2(|\omega_{jl}|^2 + |\omega_{kl}|^2)\tau_E \tau_R^3 + \cdots\right\}. \tag{46}$$

If the expansions are carried out to total order of 6 in τ_E and τ_R, very long expressions are obtained, which are *not* real in general. Similar series expansions have been given previously for the build-up of *total* multiple-quantum filtered signal amplitudes.[50–52]

The following conclusions can be drawn.

(i) All 2D amplitudes are *real* for small values of τ_E and τ_R. Under these conditions, the 2D spectra are in pure absorption, after applying a cosine Fourier transform in the t_1 dimension. Pure absorption 2D spectra are *not* obtained for single orientations in systems with $\mathcal{N}>3$, if large values of τ_E or τ_R are used.

(ii) The indirect and direct peaks have opposite signs, for small values of τ_E and τ_R.

(iii) The indirect peaks vanish for small values of the double-quantum reconversion interval τ_R.

Systems of two or three spins are special cases. The 2D amplitudes may be solved analytically, and the resulting expressions are real for all values of τ_E and τ_R. For two-spin systems, only direct double-quantum peaks exist. The relevant Liouvillian matrix elements are

$$(S_j^+ S_k^+|\hat{V}^0(\tau)|S_{jz}) = \frac{i}{2}\frac{\omega_{jk}^*}{|\omega_{jk}|}\sin(|\omega_{jk}|\tau) \tag{47}$$

leading to the double-quantum peak amplitudes

$$a_{jk\to j}^{(+2)}(\tau_E, \tau_R) = a_{jk\to j}^{(-2)}(\tau_E, \tau_R) = \tfrac{1}{4}\sin(|\omega_{jk}|\tau_E)\sin(|\omega_{jk}|\tau_R). \tag{48}$$

Since the (± 2)-quantum peak amplitudes are real and equal, the two-dimensional double-quantum spectra are in pure absorption, if a cosine Fourier transform is used in the double-quantum dimension.

For three-spin systems, the relevant Liouville space matrix elements are

$$\begin{aligned}(S_j^+ S_k^+|\hat{V}^0(\tau)|S_{jz}) &= \frac{2i\omega_{jk}^*}{3\sqrt{3}\omega_{\mathrm{rms}}^3}\sin\left(\frac{\sqrt{3}}{2}\omega_{\mathrm{rms}}\tau\right) \times\left\{|\omega_{kl}|^2 + \cos\left(\frac{\sqrt{3}}{2}\omega_{\mathrm{rms}}\tau\right) \times(|\omega_{jk}|^2 + |\omega_{jl}|^2)\right\},\\ (S_j^+ S_k^+|\hat{V}^0(\tau)|S_{lz}) &= -\frac{8i\omega_{jk}^*}{3\sqrt{3}\omega_{\mathrm{rms}}^3}\sin^3\left(\frac{\sqrt{3}}{4}\omega_{\mathrm{rms}}\tau\right) \times\cos\left(\frac{\sqrt{3}}{4}\omega_{\mathrm{rms}}\tau\right)\{|\omega_{jl}|^2 + |\omega_{kl}|^2\},\end{aligned} \tag{49}$$

where the root-mean-square recoupled interaction ω_{rms} is given by

$$\omega_{\mathrm{rms}} = \frac{1}{\sqrt{3}}(|\omega_{12}|^2 + |\omega_{13}|^2 + |\omega_{23}|^2)^{1/2}. \tag{50}$$

The two-dimensional peak amplitudes in Eq. (38) evaluate to the following expressions:

$$a_{jk\to j}^{(+2)}(\tau_E, \tau_R) = a_{jk\to j}^{(-2)}(\tau_E, \tau_R) = \frac{1|\omega_{jk}|^2}{27\omega_{\mathrm{rms}}^4}\sin(\sqrt{3}\omega_{\mathrm{rms}}\tau_E)\sin\left(\frac{\sqrt{3}}{2}\omega_{\mathrm{rms}}\tau_R\right) \times\left\{|\omega_{kl}|^2 + \cos\left(\frac{\sqrt{3}}{2}\omega_{\mathrm{rms}}\tau_R\right) \times(|\omega_{jk}|^2 + |\omega_{jl}|^2)\right\} \tag{51}$$

and

$$a_{jk\to l}^{(+2)}(\tau_E, \tau_R) = a_{jk\to l}^{(-2)}(\tau_E, \tau_R) = -\frac{4|\omega_{jk}|^2}{27\omega_{\mathrm{rms}}^4}\sin(\sqrt{3}\omega_{\mathrm{rms}}\tau_E) \times\sin^3\left(\frac{\sqrt{3}}{4}\omega_{\mathrm{rms}}\tau_R\right)\cos\left(\frac{\sqrt{3}}{4}\omega_{\mathrm{rms}}\tau_R\right) \times\{|\omega_{jl}|^2 + |\omega_{kl}|^2\}. \tag{52}$$

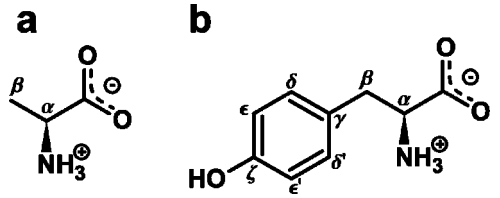

FIG. 8. Molecular structure in the samples used for the double-quantum experiments: (a) L-alanine; (b) L-tyrosine.

Similar results have been presented before for the case of $\tau_E=\tau_R$ (Refs. 17 and 53) and in the context of zero[53] and triple-quantum[54] excitation. The expressions for two-spin and three-spin systems are independent of the orientational angle γ_{MR}.

Equations (51) and (52) show that in three-spin systems, the amplitudes for the (± 2)-quantum pathways are real and equal. This implies that the two-dimensional double-quantum spectra are in pure absorption after cosine Fourier transformation in the double-quantum dimension. For systems of more than three spins, one obtains nonabsorption 2D amplitudes for single molecular orientations in the case of long τ_E or τ_R. However, simulations indicate that absorption spectra are obtained after powder averaging even in this case.

E. Double-quantum spectra

Experimental results for 98% labeled $^{13}C_3$–L-alanine [Fig. 8(a)] at $B_0=4.7$ T and a spinning frequency of $\omega_r/2\pi=11.000$ kHz are shown in Figs. 9–11. The sample was purchased from Cambridge Isotope Laboratories and used without further purification. The experiments were performed on a Chemagnetics Infinity-200 spectrometer using a filled 4 mm zirconia rotor.

The spectra were obtained using a cross-polarization contact time of 800 μs. $C14_4^{-5}$ cycles were used for both excitation and reconversion of double-quantum coherence. The excitation part of the sequence consisted of $q_E=17$ cycles, which corresponds to an excitation time of $\tau_E=441.5\,\mu$s. The evolution interval t_1 was incremented in steps of 21.74 μs. Continuous wave decoupling was used with the proton nutation frequency 100 kHz during the $C14_4^{-5}$ sequences, and 74 kHz during the evolution and acquisition intervals. The signal in the t_1 dimension was apodized with a $\cos^2$ function and converted into the time domain using a cosine Fourier transform.

Figure 9(a) shows the experimental 2D double-quantum spectrum for a reconversion interval $\tau_R=207.8\,\mu$s. Note the absence of the indirect double-quantum peaks for this short value of the reconversion interval. Figure 10(a) shows experimental results for a long reconversion interval $\tau_R=1168.8\,\mu$s. The spectrum displays strong direct and indirect peaks of both signs. In both cases all peaks are in pure absorption phase, as predicted. Note that the negative sign of a peak does *not* indicate that it is indirect.

Figures 9(b) and 10(b) show numerically exact simulations of the two-dimensional spectra, using the spin interaction parameters given in Ref. 55. The simulations mimic the experiments as closely as possible only assuming rectangular pulses and neglect of relaxation and were performed using the COMPUTE algorithm[55,56] in the t_2 dimension for optimal computational efficiency. Agreement with experiments is good, with the exception of the peak amplitudes. We attribute these discrepancies to relaxation effects in the experimental system (see below). The simulations in Fig. 10(b) employ an rf field with an amplitude equal to 99.4% of the nominal value. The simulation using the nominal rf value displays small phase distortions.

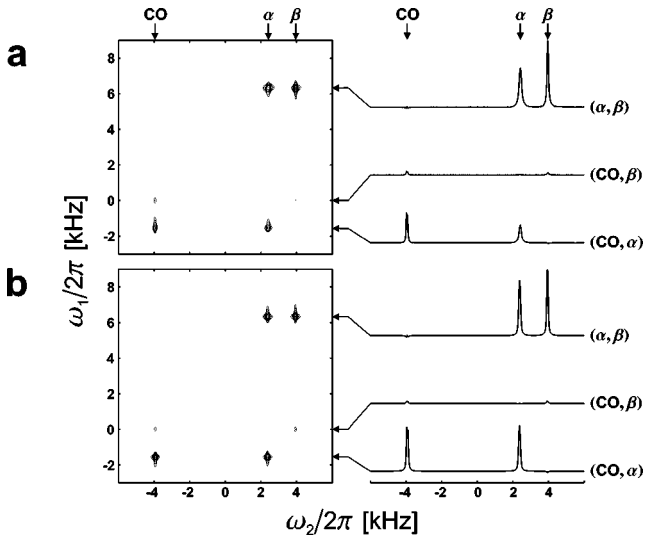

FIG. 9. (a) Experimental 2D double-quantum ^{13}C spectra of 98% $^{13}C_3$–L-alanine, obtained using the pulse sequence in Fig. 7 with $\tau_E=441.5\,\mu$s and $\tau_R=207.8\,\mu$s. Note the absorption mode spectral peak shapes and the absence of indirect double-quantum peaks. (b) Accurate numerical simulations using the known geometry of the three-spin system and the simulation parameters in Ref. 55. Powder averaging was performed using 1154 orientations Ω_{MR}, chosen according to the ZCW scheme (Ref. 62).

Figure 11 shows the measured integrals of the 2D peaks as a function of the reconversion interval τ_R, with the excitation interval remaining fixed at the value $\tau_E=441.5\,\mu$s.

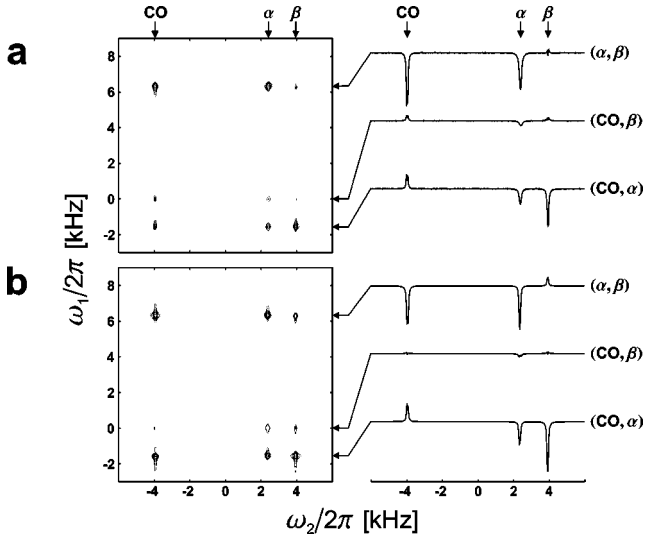

FIG. 10. As in Fig. 9, but with $\tau_E=441.5\,\mu$s and $\tau_R=1168.8\,\mu$s. Negative peaks denoted by gray contour lines.

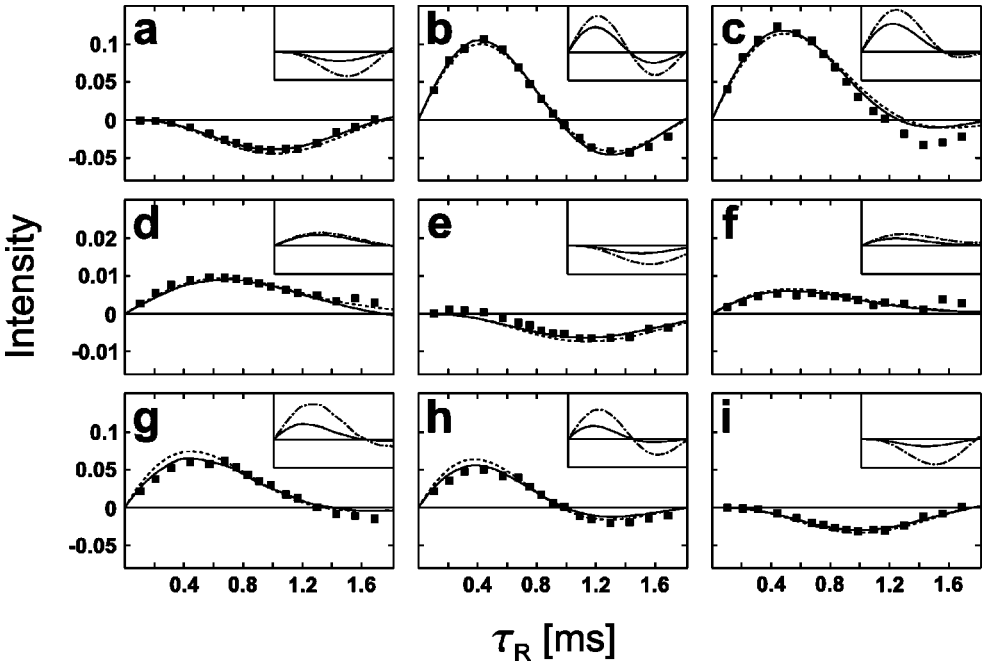

FIG. 11. Main plots: Symbols: Experimental integrals of the 9 spectral peaks in the 2D double-quantum ^{13}C spectra of 98% $^{13}C_3$–L-alanine, obtained using the pulse sequence in Fig. 7 as a function of the reconversion interval τ_R. The excitation interval was fixed at $\tau_E = 441.5\ \mu s$. The plots show the amplitudes of peaks with the following frequency coordinates (ω_1, ω_2): (a) $(\omega_\alpha^{iso}+\omega_\beta^{iso}, \omega_{CO}^{iso})$; (b) $(\omega_\alpha^{iso}+\omega_\beta^{iso}, \omega_\alpha^{iso})$; (c) $(\omega_\alpha^{iso}+\omega_\beta^{iso}, \omega_\beta^{iso})$; (d) $(\omega_{CO}^{iso}+\omega_\beta^{iso}, \omega_{CO}^{iso})$; (e) $(\omega_{CO}^{iso}+\omega_\beta^{iso}, \omega_\alpha^{iso})$; (f) $(\omega_{CO}^{iso}+\omega_\beta^{iso}, \omega_\beta^{iso})$; (g) $(\omega_{CO}^{iso}+\omega_\alpha^{iso}, \omega_{CO}^{iso})$; (b) $(\omega_{CO}^{iso}+\omega_\alpha^{iso}, \omega_\alpha^{iso})$; (i) $(\omega_{CO}^{iso}+\omega_\alpha^{iso}, \omega_\beta^{iso})$. Solid lines: accurate numerical simulations of the amplitudes using the known geometry and J couplings and including damping. Dashed lines: Analytical solutions given in Eqs. (51) and (52) including damping. In both cases the same powder averaging as in Fig. 9(b) was performed. The phenomenological relaxation time constants used in Eq. (54) are given by (a)–(c); $T_{\alpha\beta,CO}=1.34$ ms, $T_{\alpha\beta,\alpha}=2.34$ ms, $T_{\alpha\beta,\beta}=2.28$ ms; (d)–(f), $T_{\alpha CO,CO}=26.1$ ms, $T_{\alpha CO,\alpha}=1.57$ ms, $T_{\alpha CO,\beta}=1.58$ ms; (g)–(i), $T_{CO\beta,CO}=1.18$ ms, $T_{CO\beta,\alpha}=1.05$ ms, $T_{CO\beta,\alpha}=1.22$ ms. Insets: solid lines: simulations using damping. Dotted–dashed lines: simulations without damping. Note the vertical scale of (d)–(f).

The slow initial build up of the indirect peaks is visually obvious. Effects involving all three spins are already evident for very short reconversion intervals.

The solid lines in the figure are the results of accurate three-spin simulations, using the spin interaction parameters given in Ref. 55. These simulations use a calculation of the two-dimensional double-quantum amplitudes according to

$$a_{jk\to l}^{(\pm 2)\prime}(\tau_E,\tau_R) = -\Re\sum_m (S_{lz}|\hat{U}(t_R^1,t_R^0)|S_j^{\pm}S_k^{\pm})' \times (S_j^{\pm}S_k^{\pm}|\hat{U}(t_E^1,t_E^0)|S_{mz})', \tag{53}$$

where $\hat{U}(t^1,t^0)$ is the numerical calculated propagator, including all spin interactions and the evolution interval is set to zero ($t_E^1=t_R^0$). In practice the matrix elements were calculated in Hilbert space. This equation corresponds to the average Hamiltonian equation [Eq. (38)], but incorporating a phenomenological correction for relaxation during the multiple pulse sequence. The modified matrix elements are given by

$$(S_j^{\pm}S_k^{\pm}|\hat{U}(t_E^1,t_E^0)|S_{mz})' = (S_j^{\pm}S_k^{\pm}|\hat{U}(t_E^1,t_E^0)|S_{mz})e^{-\tau/T_{jk,m}},$$
$$(S_{lz}|\hat{U}(t_R^1,t_R^0)|S_j^{\pm}S_k^{\pm})' = (S_{lz}|\hat{U}(t_R^1,t_R^0)|S_j^{\pm}S_k^{\pm})e^{-\tau/T_{jk,l}}. \tag{54}$$

Each of the nine independent time constants $T_{jk,l}$ with $j,k,l=CO,\alpha,\beta$ denoting the corresponding ^{13}C site, corresponds to the transfer of an initial z-magnetization component to an individual double-quantum coherence. In practice, the nine time constants may be divided into three groups of three. Each group of three may be estimated simultaneously by a least square fit to three experimental curves. For example, $T_{\alpha\beta,CO}$, $T_{\alpha\beta,\alpha}$, and $T_{\alpha\beta,\beta}$ are estimated by fitting $a_{\alpha\beta\to CO}^{(\pm 2)\prime}$, $a_{\alpha\beta\to\alpha}^{(\pm 2)\prime}$, and $a_{\alpha\beta\to\beta}^{(\pm 2)\prime}$ to the experimental results in Figs. 11(a)–11(c). Similar estimations can be done for the two remaining groups of damping time constants. In practice, the quality of the fit was not very sensitive to the precise value of these relaxation time constants.

The dashed lines in Fig. 11 are given by the analytical formula Eq. (51) and Eq. (52), but also use the phenomenological damping factors. The same damping time constants are used as for the solid lines.

The inset plots in Fig. 11 compare the exact numerical simulations with and without damping. The solid line corresponds to the damped curves in the main plot, while the dotted–dashed line represents the simulations without damping.

We have compared these simulations with full two-dimensional spectral simulations shown in Figs. 9(b) and 10(b). The difference between the two simulation results is insignificant.

The agreement between the exact numerical simulations, analytical results, and the experimental amplitudes is good. The deviations are largest for double-quantum peaks involving CO, which is due to its large CSA. The plotted experimental amplitudes only contain the centerband contributions, and slightly underestimate the full magnetization amplitudes.

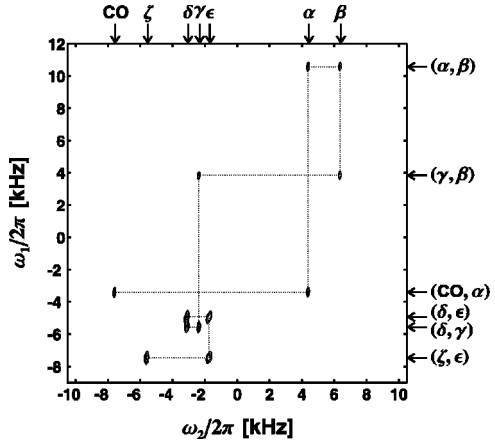

FIG. 12. Experimental 2D double-quantum ^{13}C spectrum of [98%–U–^{13}C]–L-tyrosine, at a field of $B_0=9.4$ T and a spinning frequency of $\omega_r/2\pi=20.000$ kHz, obtained using the pulse sequence in Fig. 7 with the supercycle SC14 for excitation and reconversion of double-quantum coherence. The excitation and reconversion intervals were $\tau_E=400.1$ μs and $\tau_R=100.0$ μs. The assignments of the double-quantum coherences to the molecular site pairs are indicated along the right-hand axis.

Figure 12 shows an experimental 2D double-quantum spectrum of [98%–U–^{13}C]–L-tyrosine [Fig. 8(b)] at $B_0=9.4$ T and a spinning frequency of $\omega_r/2\pi=20.000$ kHz. In this case the supercycled sequence SC14 was used. The excitation part of the sequence consisted of $q_E=28$ cycles, i.e., the excitation sequence was given by $C14_4^5\cdot[\Pi_0^{-1}\cdot C14_4^{-5}\cdot\Pi_0]_{\pi/7}$. The reconversion part of the sequence consisted of $q_R=7$, i.e., seven elements of $[C14_4^5]_\pi$. The excitation and reconversion time intervals were given by $\tau_E=400.1$ μs and $\tau_R=100.0$ μs. The sample was purchased from Cambridge Isotope Laboratories and used without further purification. The experiments were performed on a Chemagnetics Infinity-400 spectrometer using a filled 3.2 mm zirconia rotor. The spectra were obtained using a cross-polarization contact time of 2.5 ms. The evolution interval t_1 was incremented in steps of 10 μs. Continuous wave decoupling was used during SC14 with a proton nutation frequency of 227 kHz. TPPM decoupling[57] was used during the evolution interval t_1 and the acquisition. The proton nutation frequency was 96 kHz. The signal in the t_1 dimension was apodized with a $\cos^2$ function and converted into the time domain using a cosine transform. The experimental 2D spectrum permits a straightforward assignment of the ^{13}C peaks, as in the liquid state 2D-INADEQUATE experiment.[32,33] A slight nonequivalence of the δ, δ' and ϵ, ϵ' sites may be discerned.

IV. CONCLUSIONS

The results given in this paper may be summarized as follows: (i) It is possible to develop a general theory of recoupling in magic-angle-spinning solids, exploiting synchronized helical modulations of the space and spin parts of the nuclear magnetic interactions. The average Hamiltonian properties of such sequences may be formulated in terms of the three symmetry numbers for the pulse sequence. (ii) These principles may be applied to the problem of spin system recoupling at high spinning frequencies. A sequence has been demonstrated which employs an exceptional low ratio of rf field to spinning frequency while still being robust with respect to rf amplitude errors. (iii) This class of sequences may be compensated with respect to chemical shift effects by employing a supercycle scheme. (iv) The dynamics of recoupled multiple-spin systems have been thoroughly analyzed in the context of double-quantum spectroscopy at high MAS frequencies. Good agreement is obtained between the experimental spectra and analytical results as well as numerically exact simulations, in the case of a three-spin system of known geometry.

The principles of pulse sequence construction described here are very general and may be applied to a number of other problems in magic-angle-spinning NMR. Applications to heteronuclear decoupling have been described elsewhere.[35] In addition, the symmetries $C3_1^0$ and $C4_1^0$ have been used for selection of isotropic Hamiltonians[58] and homonuclear decoupling,[59] respectively. These principles are immediately predictable from the symmetry rules described in the current paper. Generalized symmetry rules which allow the treatment of heteronuclear pulse sequences will be described elsewhere.

The $C14_4^5$ sequence described in this paper is not a unique solution for recoupling at high spinning frequency. As indicated in Table I, a very large number of useful CN_n^ν symmetries exist, and each symmetry permits great freedom in the choice of the elemental cycle. In addition, it is possible to construct sequences with the same interaction frame symmetry as CN_n^ν sequences, but with elements consisting of z-rotations instead of cycles. This additional degree of freedom has been discussed in the context of TPPM decoupling[57] in Ref. 35. The results presented here should be regarded as defining a framework guiding the search for optimal sequences. In the end, the choice of the basic element and the type of symmetry must be guided by more detailed considerations such as the particular form of the recoupled Hamiltonian, and the properties of the higher-order terms. The solutions discussed in this paper is only one of a huge number of possibilities. Furthermore, new symmetry classes with different selection rules have recently been described.[40]

Two-dimensional spectroscopy of multiple-spin systems at high spinning frequencies is expected to become increasingly important, especially in the solid-state NMR of heavily labeled biomolecules. The good agreement of the experimental three-spin dynamics with the theoretical curves, as shown in Fig. 11, bodes well for the precise control of spin dynamics in such experiments.

ACKNOWLEDGMENTS

The research was supported by the Göran Gustafson Foundation for Research in the Natural Sciences and Medicine, and the Swedish Natural Science Foundation. A.B. has been supported by the Marie Curie Research Training Grant ERBFMBICT961439 from the European Union. We thank O. G. Johannessen for experimental help and A. Sebald and S. Dusold for discussions.

APPENDIX A: SUPERCYCLED CN_n^ν SEQUENCES

The spin Hamiltonian in the presence of a rotor synchronized rf pulse sequence is given by

$$H(t)=H_{\rm int}(t)+H_{\rm rf}(t), \tag{A1}$$

where the internal spin Hamiltonian $H_{\rm int}(t)$ is time dependent because of the sample rotation, while the rf spin Hamiltonian $H_{\rm rf}(t)$ is time dependent because of the modulation of the rf fields. It is convenient to analyze the spin dynamics in the interaction frame of the rf field, i.e.,

$$\tilde{H}(t)=W(t)^\dagger H_{\rm int}(t)W(t), \tag{A2}$$

where the frame transformation operator $W(t)$ solves the equations

$$\frac{d}{dt}W(t)=-iH_{\rm rf}(t)W(t), \tag{A3}$$

$$W(t^0)=\mathbb{1}. \tag{A4}$$

These equations maintain a notational distinction between operators which connect states at two different time points (''propagators'') and those that depend on one time point.[60] The propagator under the interaction frame Hamiltonian over the duration T of the pulse sequence (starting at time point t^0) is expressed in terms of an effective Hamiltonian

$$\tilde{U}(T+t^0,t^0)=\exp\{-i\bar{H}T\}, \tag{A5}$$

where $\bar{H}$ is usually approximated as a truncated Magnus expansion

$$\bar{H}\cong\bar{H}^{(1)}+\bar{H}^{(2)} \tag{A6}$$

with

$$\bar{H}^{(1)}=T^{-1}\int_{t^0}^{t^0+T}dt\,\tilde{H}(t), \tag{A7}$$

$$\bar{H}^{(2)}=(2iT)^{-1}\int_{t^0}^{t^0+T}dt'\int_{t^0}^{t'}dt[\tilde{H}(t'),\tilde{H}(t)]. \tag{A8}$$

The internal part of the spin Hamiltonian may be expressed using terms with different spherical rank λ for rotations of the spin polarizations

$$H_{\rm int}(t)=\sum_\lambda H_\lambda(t), \tag{A9}$$

where $H_\lambda(t)$ is proportional to the irreducible spherical spin operator $T_{\lambda 0}$. For example, chemical shift terms (both isotropic and anisotropic) have $\lambda=1$, while homonuclear dipole–dipole coupling terms have $\lambda=2$. The Magnus expansion terms may then be written

$$\bar{H}^{(1)}=\sum_\lambda \bar{H}_\lambda^{(1)}, \tag{A10}$$

$$\bar{H}^{(2)}=\sum_{\lambda_2,\lambda_1}\bar{H}_{\lambda_2\times\lambda_1}^{(2)}, \tag{A11}$$

where

$$\bar{H}_\lambda^{(1)}=T^{-1}\int_{t^0}^{t^0+T}dt\,\tilde{H}_\lambda(t), \tag{A12}$$

$$\bar{H}_{\lambda_2\times\lambda_1}^{(2)}=(2iT)^{-1}\int_{t^0}^{t^0+T}dt'\int_{t^0}^{t'}dt[\tilde{H}_{\lambda_2}(t'),\bar{H}_{\lambda_1}(t)], \tag{A13}$$

and

$$\tilde{H}_\lambda(t)=W(t)^\dagger H_\lambda(t)W(t). \tag{A14}$$

The symmetry rules given in Eq. (8) may be used to engineer sequences with desirable properties for $\bar{H}^{(1)}$. For example, the chemical shift anisotropy components of $\bar{H}^{(1)}$ vanish for the symmetries $C7_2^1$, $C14_4^5$, etc., as given in Table I. It is also possible to predict the destruction of a large number of cross terms of the form $\bar{H}_{2\times1}^{(2)}$.[35] However, the remaining high-order terms cause an undesirable interference between dipole–dipole recoupling and chemical shift anisotropy.

In order to see how to eliminate such terms, compare now two sequences with opposite spin winding number ν, i.e., CN_n^ν and $CN_n^{-\nu}$. For brevity, these sequences are denoted (C^+) and (C^-). The rf spin Hamiltonians for these two sequences are related through

$$H_{\rm rf}(C^+)=R_x(\pi)H_{\rm rf}(C^-)R_x(\pi)^\dagger, \tag{A15}$$

where $R_x(\pi)=\exp\{-i\pi S_x\}$. This equation assumes that all rf phases are reversed in sign between the two sequences, including any internal phases within the C elements (this latter condition is unnecessary if the C elements only contain 0 and π phase shifts). The frame transformation operators for the two sequences at corresponding points of time are therefore related through

$$W(C^+;t)=R_x(\pi)W(C^-;t)R_x(\pi)^\dagger. \tag{A16}$$

The interaction frame spin Hamiltonians for an interaction of spin rank λ are related by

$$\begin{aligned}\tilde{H}_\lambda(C^+;t)&=W(C^+;t)^\dagger H_\lambda(t)W(C^+;t)\\&=R_x(\pi)W(C^-;t)^\dagger R_x(\pi)^\dagger H_\lambda(t)\\&\quad\times R_x(\pi)W(C^-;t)R_x(\pi)^\dagger\\&=(-1)^\lambda R_x(\pi)\tilde{H}_\lambda(C^-;t)R_x(\pi)^\dagger.\end{aligned} \tag{A17}$$

The last line follows from the transformation property

$$R_x(\pi)T_{\lambda0}R_x(\pi)^\dagger=(-1)^\lambda T_{\lambda0}. \tag{A18}$$

It follows that the average Hamiltonian terms for the two sequences are related by

$$\bar{H}_\lambda^{(1)}(C^+)=(-1)^\lambda R_x(\pi)\bar{H}_\lambda^{(1)}(C^-)R_x(\pi)^\dagger, \tag{A19}$$

$$\bar{H}_{\lambda_2\times\lambda_1}^{(2)}(C^+)=(-1)^{\lambda_2+\lambda_1}R_x(\pi)\bar{H}_{\lambda_2\times\lambda_1}^{(2)}(C^-)R_x(\pi)^\dagger. \tag{A20}$$

Equation (A19) shows for example, that two CN_n^ν sequences with opposite signs of ν cannot be concatenated without destroying the desirable γ-encoding of the double-quantum recoupling.

Now consider a hypothetical situation in which the $CN_n^{-\nu}$ sequence is bracketed by two infinitely strong ideal π pulses of phase 0. Denote this bracketed sequence by the

symbol ($\Pi C^{-}\Pi$). The effect of the π pulse is to rotate the overall propagator by the angle π around the x axis, which leads to the relationships:

$$\bar{H}_{\lambda}^{(1)}(C^{+})=(-1)^{\lambda}\bar{H}_{\lambda}^{(1)}(\Pi C^{-}\Pi), \tag{A21}$$

$$\bar{H}_{\lambda_2\times\lambda_1}^{(2)}(C^{+})=(-1)^{\lambda_2+\lambda_1}\bar{H}_{\lambda_2\times\lambda_1}^{(2)}(\Pi C^{-}\Pi). \tag{A22}$$

Now suppose that the CN_n^{ν} sequence and the ''bracketed'' $CN_n^{-\nu}$ sequence are concatenated to build a supercycle. This idealized supercycle is denoted ($C^{+}\Pi C^{-}\Pi$). The first order average Hamiltonian term for the supercycle is given by

$$\bar{H}_{\lambda}^{(1)}(C^{+}\Pi C^{-}\Pi)=\tfrac{1}{2}\bar{H}_{\lambda}^{(1)}(C^{+})+\tfrac{1}{2}\bar{H}_{\lambda}^{(1)}(\Pi C^{-}\Pi). \tag{A23}$$

This has the property

$$\bar{H}_{\lambda}^{(1)}(C^{+}\Pi C^{-}\Pi)=\begin{cases}0 & \text{for } \lambda=\text{odd},\\ \bar{H}_{\lambda}^{(1)}(C^{+}) & \text{for } \lambda=\text{even}.\end{cases} \tag{A24}$$

It follows that this type of supercycle preserves the first order average Hamiltonian for $\lambda=2$ terms (such as dipolar couplings), while destroying $\lambda=1$ terms (such as chemical shifts). These are desirable properties for homonuclear recoupling sequences.

For the second-order term, the corresponding calculation gives

$$\begin{aligned}\bar{H}_{\lambda_2\times\lambda_1}^{(2)}(C^{+}\Pi C^{-}\Pi)=&\ \tfrac{1}{2}\bar{H}_{\lambda_2\times\lambda_1}^{(2)}(C^{+})\\ &-\frac{i}{4}[\bar{H}_{\lambda_2}^{(1)}(\Pi C^{-}\Pi),\bar{H}_{\lambda_1}^{(1)}(C^{+})]\\ &+\tfrac{1}{2}\bar{H}_{\lambda_2\times\lambda_1}^{(2)}(\Pi C^{-}\Pi).\end{aligned} \tag{A25}$$

For most of the interesting cross terms, the individual sequences are designed so as to eliminate the corresponding $\bar{H}_{\lambda}^{(1)}$ terms, so that the commutator may be neglected. This is true, for example, for the cross terms involving the chemical shift anisotropy, in the case of $C7_2^1$ and $C14_4^5$ sequences. Under these conditions, the theorem for the second order cross terms is

$$\bar{H}_{\lambda_2\times\lambda_1}^{(2)}(C^{+}\Pi C^{-}\Pi)=\begin{cases}0 & \text{for } \lambda_2+\lambda_1=\text{odd},\\ \bar{H}_{\lambda_2\times\lambda_1}^{(2)}(C^{+}) & \text{for } \lambda_2+\lambda_1=\text{even}.\end{cases} \tag{A26}$$

This theorem shows that the second order cross term involving the chemical shift anisotropy ($\lambda=1$) and homonuclear dipole–dipole coupling ($\lambda=2$) vanishes for the ($C^{+}\Pi C^{-}\Pi$) supercycle.

In practice, it is not possible to implement the idealized short π pulses required by the ($C^{+}\Pi C^{-}\Pi$) supercycle. However *cyclic permutation* of a π pulse achieves an approximately similar effect.[61] A small additional phase shift of the pulse sequence is used to compensate for the finite time interval spanned by the permuted element. The symmetry theorems given in Eqs. (A24) and (A26) apply only approximately to supercycles employing cyclically permuted elements, but accurate simulations indicate that the approximation is reasonable.

The residual error terms are reduced further by repeating the entire sequence with a π phase shift, which generates the SC14 supercycle written in Eq. (12).

APPENDIX B: SYMMETRIES OF DOUBLE-QUANTUM SPECTRAL AMPLITUDES

In this appendix, we prove Eqs. (41) and (44), which are important for the calculation of double-quantum spectral peak amplitudes.

First consider the properties of the superoperator $\hat{V}$, given by

$$\hat{V}=\exp\{-i\hat{\bar{H}}^{\text{comm}}\tau\}. \tag{B1}$$

Here $\hat{\bar{H}}^{\text{comm}}$ is the commutation superoperator of the first-order average Hamiltonian

$$\hat{\bar{H}}^{\text{comm}}|A)=|[\bar{H}^{(1)},A]). \tag{B2}$$

The superoperator $\hat{V}$ is a ''sandwich superoperator,''[49] with the property

$$\hat{V}|A)=|VAV^{\dagger}), \tag{B3}$$

where the propagator V is given by

$$V=\exp\{-i\tau\bar{H}^{(1)}\}. \tag{B4}$$

The following reasoning may be made:

$$\begin{aligned}(A|\hat{V}|B)^{*}&=(A|VBV^{\dagger})^{*}\\ &=\text{Tr}\{(A^{\dagger}VBV^{\dagger})^{\dagger}\}\\ &=\text{Tr}\{VB^{\dagger}V^{\dagger}A\}\\ &=\text{Tr}\{AVB^{\dagger}V^{\dagger}\}=(A^{\dagger}|\hat{V}|B^{\dagger}).\end{aligned} \tag{B5}$$

Equation (41) follows by applying Eq. (B5), noting that $S_{lz}^{\dagger}=S_{lz}$ and $(S_j^{+})^{\dagger}=S_j^{-}$.

In order to prove Eq. (44), suppose that an operator R exists with the following properties:

$$\begin{aligned}&RR^{\dagger}=1,\\ &RVR^{\dagger}=V^{\dagger},\\ &RAR^{\dagger}=A,\\ &RBR^{\dagger}=-B.\end{aligned} \tag{B6}$$

The following reasoning may be developed:

$$\begin{aligned}(A|\hat{V}|B)^{*}&=(A^{\dagger}|\hat{V}|B^{\dagger})\\ &=\text{Tr}\{AVB^{\dagger}V^{\dagger}\}\\ &=\text{Tr}\{RAR^{\dagger}RVR^{\dagger}RBR^{\dagger}RV^{\dagger}R^{\dagger}\}\\ &=-\text{Tr}\{AV^{\dagger}BV\}\\ &=-\text{Tr}\{BVAV^{\dagger}\}=-(B^{\dagger}|\hat{V}|A).\end{aligned} \tag{B7}$$

This equation establishes the symmetry relationship in Eq. (44), if the following identifications are made $A=S_{lz}$, $B=S_j^{\pm}S_k^{\pm}$.

It remains to identify an operator R with the properties in Eq. (B6). If the average Hamiltonian has the form of Eq.

(17), and the J couplings are ignored in Eq. (18), then the operator

$$R = \exp\left\{ -i \frac{\pi}{2} S_z \right\} \tag{B8}$$

has the appropriate properties.

[1] D. P. Raleigh, M. H. Levitt, and R. G. Griffin, Chem. Phys. Lett. **146**, 71 (1988).
[2] Z.-H. Gan and D. M. Grant, Mol. Phys. **67**, 1419 (1989).
[3] M. H. Levitt, D. P. Raleigh, F. Creuzet, and R. G. Griffin, J. Chem. Phys. **90**, 6347 (1990).
[4] T. Karlsson and M. Levitt, J. Chem. Phys. **109**, 5493 (1998).
[5] M. Helmle *et al.*, J. Magn. Reson. **140**, 379 (1999).
[6] T. Karlsson, M. Edén, H. Luthman, and M. H. Levitt, J. Magn. Reson. (in press).
[7] K. Nomura, K. Takegoshi, T. Terao, K. Uchida, and M. Kainosho, J. Am. Chem. Soc. **121**, 4064 (1999).
[8] T. Gullion and J. Schaefer, Adv. Magn. Reson. **13**, 57 (1989).
[9] R. Tycko and G. Dabbagh, J. Am. Chem. Soc. **113**, 9444 (1991).
[10] D. M. Gregory *et al.*, Chem. Phys. Lett. **246**, 654 (1995).
[11] M. Baldus, M. Tomaselli, B. Meier, and R. R. Ernst, Chem. Phys. Lett. **230**, 329 (1994).
[12] M. Baldus and B. H. Meier, J. Magn. Reson. **128**, 172 (1997).
[13] N. C. Nielsen, H. Bildsøe, H. J. Jakobsen, and M. H. Levitt, J. Chem. Phys. **101**, 1805 (1994).
[14] Y. K. Lee *et al.*, Chem. Phys. Lett. **242**, 304 (1995).
[15] C. M. Rienstra *et al.*, J. Am. Chem. Soc. **120**, 10602 (1998).
[16] M. Hohwy, H. J. Jakobsen, M. Edén, M. H. Levitt, and N. C. Nielsen, J. Chem. Phys. **108**, 2686 (1998).
[17] M. Hohwy, C. M. Rienstra, C. P. Jaroniec, and R. G. Griffin, J. Chem. Phys. **110**, 7983 (1999).
[18] Y. Ishii, T. Terao, and M. Kainosho, Chem. Phys. Lett. **265**, 133 (1996).
[19] X. Feng *et al.*, Chem. Phys. Lett. **257**, 314 (1996).
[20] X. Feng *et al.*, J. Am. Chem. Soc. **119**, 12006 (1997).
[21] M. Hong, J. D. Gross, and R. G. Griffin, J. Phys. Chem. B **101**, 5869 (1997).
[22] P. R. Costa, J. D. Gross, M. Hong, and R. G. Griffin, Chem. Phys. Lett. **280**, 95 (1997).
[23] T. Fujiwara, T. Shimomura, and H. Akutsu, J. Magn. Reson. **124**, 147 (1997).
[24] Y. Ishii *et al.*, Solid State Nucl. Magn. Reson. **11**, 169 (1998).
[25] X. Feng *et al.*, J. Am. Chem. Soc. **119**, 6853 (1997).
[26] A. E. Bennett, J. H. Ok, and R. G. Griffin, J. Chem. Phys. **96**, 8624 (1992).
[27] W. A. Dollase *et al.*, J. Am. Chem. Soc. **119**, 3807 (1997).
[28] T. S. Balaban, A. R. Holzwarth, K. Schaffner, G.-J. Boender, and H. J. M. de Groot, Macromolecules **31**, 7404 (1995).
[29] T. A. Egorova-Zachernyuk, B. van Rossum, G.-J. Boender, and H. J. M. de Groot, Biochemistry **36**, 7513 (1997).
[30] L. Braunschweiler and R. R. Ernst, J. Magn. Reson. **53**, 521 (1983).
[31] A. Bax, R. Freeman, and S. P. Kempsell, J. Am. Chem. Soc. **102**, 4849 (1980).
[32] A. Bax, R. Freeman, and T. Frenkiel, J. Am. Chem. Soc. **103**, 2102 (1981).
[33] A. Bax, R. Freeman, T. Frenkiel, and M. H. Levitt, J. Magn. Reson. **43**, 478 (1981).
[34] M. M. Maricq and J. S. Waugh, J. Chem. Phys. **70**, 3300 (1979).
[35] M. Edén and M. H. Levitt, J. Chem. Phys. **111**, 1511 (1999).
[36] W. Magnus, Commun. Pure Appl. Math. **7**, 649 (1954).
[37] We employ an indexing of the Magnus expansion starting at one. The older literature on average Hamiltonian theory uses indices which are one less than those given here.
[38] A. Brinkmann, M. Edén, X. Feng, H. Luthman, L. Eriksson, A. Gräslund, O. N. Antzutkin, and M. H. Levitt, 39th Experimental NMR Conference, Asilomar, CA, 1998.
[39] R. R. Ernst, G. Bodenhausen, and A. Wokaun, *Principles of Nuclear Magnetic Resonance in One and Two Dimensions*, 5th ed. (Clarendon, Oxford, 1988).
[40] M. Carravetta, M. Edén, X. Zhao, A. Brinkmann, and M. H. Levitt, Chem. Phys. Lett. (in press).
[41] T. Karlsson, A. Brinkmann, P. J. E. Verdegem, J. Lugtenburg, and M. H. Levitt, Solid State Nucl. Magn. Reson. **14**, 43 (1998).
[42] M. H. Levitt, J. Magn. Reson. **126**, 164 (1997).
[43] M. H. Levitt and O. G. Johannessen, J. Magn. Reson. **142**, 190 (2000).
[44] A. McDermott, T. Polenova, G. Montelione, K. Zilm, E. Paulsen, R. Martin, and G. Coker, 40th Experimental NMR Conference, Orlando, FL, 1999.
[45] G. Metz, X. Wu, and S. O. Smith, J. Magn. Reson., Ser. A **110**, 219 (1994).
[46] A. Brinkmann, M. Edén, and M. H. Levitt (unpublished).
[47] M. Hong, J. Magn. Reson. **136**, 86 (1999).
[48] D. A. Varshalovich, A. N. Moskalev, and V. K. Khersonskii, *Quantum Theory of Angular Momentum* (World Scientific, Singapore, 1988).
[49] J. Jeener, Adv. Magn. Reson. **10**, 1 (1982).
[50] Y. Yen and A. Pines, J. Chem. Phys. **78**, 3579 (1983).
[51] J. Baum, M. Munowich, A. N. Garroway, and A. Pines, J. Chem. Phys. **83**, 2015 (1985).
[52] Y. Ba and W. S. Veeman, Isr. J. Chem. **32**, 173 (1992).
[53] A. K. Roy and K. K. Gleason, J. Magn. Reson., Ser. A **120**, 139 (1996).
[54] M. Edén and M. H. Levitt, Chem. Phys. Lett. **293**, 173 (1998).
[55] M. H. Levitt and M. Edén, Mol. Phys. **95**, 879 (1998). Table I of this paper contains two misprints: The signs of $\alpha_{PM}(C_\beta)$ and $b(C_\alpha - C_\beta)$ should be reversed.
[56] M. Edén, Y. K. Lee, and M. H. Levitt, J. Magn. Reson., Ser. A **120**, 56 (1996).
[57] A. E. Bennett, C. M. Rienstra, M. Auger, K. V. Lakshmi, and R. G. Griffin, J. Chem. Phys. **103**, 6951 (1995).
[58] M. Baldus and B. H. Meier, J. Magn. Reson. **121**, 65 (1996).
[59] D. E. Demco, S. Hafner, and H. W. Spiess, J. Magn. Reson., Ser. A **116**, 36 (1995).
[60] J. Jeener, Bull. Magn. Reson. **16**, 35 (1994).
[61] M. H. Levitt, R. Freeman, and T. Frenkiel, Adv. Magn. Reson. **11**, 47 (1983).
[62] V. B. Cheng, H. H. Suzukawa, and M. Wolfsberg, J. Chem. Phys. **59**, 3992 (1973).